

INTERNATIONAL UNION OF PURE AND APPLIED CHEMISTRY

ANALYTICAL CHEMISTRY DIVISION
COMMISSION ON RADIOCHEMISTRY AND NUCLEAR TECHNIQUES*

CRITICAL REVIEW OF ANALYTICAL APPLICATIONS OF MÖSSBAUER SPECTROSCOPY ILLUSTRATED BY MINERALOGICAL AND GEOLOGICAL EXAMPLES

(IUPAC Technical Report)

E. KUZMANN^{1,‡}, S. NAGY², AND A. VÉRTES¹

¹Laboratory of Nuclear Techniques in Structural Chemistry, Hungarian Academy of Sciences, Budapest, Hungary; ²Department of Nuclear Chemistry, Eötvös Loránd University, Budapest, Hungary

*Membership of the Commission during the preparation of this report (1995–2001) was as follows:

Titular Members: V. P. Kolotov (Chairman, Russia); P. Benes (Secretary, Czech Republic); C. Chai (P.R. China); H. W. Gaggeler (Switzerland); J. V. Kratz (Germany); **Associate Members:** C. H. Collins (Brazil); F. De Corte (Belgium); J. de Goeij (Netherlands); Yu. Nagame (Japan); A. Vertes (Hungary); P. Vitorge (France); A. R. Ware (UK); S. W. Yates (USA); **National Representatives:** N. E. Holden (USA); Sc. F. Macasek (Slovakia); B. F. Myasoedov (Russia); N. B. Kirn (S. Korea); S. Nagy (Hungary); J. M. Peixoto de Cabral (Portugal); A. Plonka (Poland); A. V. R. Reddy (India); C. Testa (Italy); P. Nedkov (Bulgaria).

[‡]Corresponding author: E-mail: kuzmann@ludens.elte.hu

Republication or reproduction of this report or its storage and/or dissemination by electronic means is permitted without the need for formal IUPAC permission on condition that an acknowledgment, with full reference to the source, along with use of the copyright symbol ©, the name IUPAC, and the year of publication, are prominently visible. Publication of a translation into another language is subject to the additional condition of prior approval from the relevant IUPAC National Adhering Organization.

Critical review of analytical applications of Mössbauer spectroscopy illustrated by mineralogical and geological examples

(IUPAC Technical Report)

Abstract: We have developed a new terminology for Mössbauer pattern analysis in order to enhance the performance of qualitative analysis by Mössbauer spectroscopy. In this approach, Mössbauer parameters are considered as a function of a number of externally adjusted experimental parameters at which the spectrum has been recorded. The basis of analytical classification is the microenvironment, which is determined by an assembly of atoms causing the same hyperfine interactions at one particular class of the Mössbauer probe atoms. Since Mössbauer spectroscopy measures hyperfine interactions very sensitively, the microenvironment presents itself as a fundamental concept for analytical purposes. Our approach can also help to systematize the Mössbauer data for the identification of individual physicochemical species from the corresponding patterns present in the spectrum.

CONTENTS

INTRODUCTION

1. BASIC PRINCIPLES OF MÖSSBAUER SPECTROSCOPY
 - 1.1 Mössbauer parameters
 - 1.2 Dependence of the Mössbauer parameters on experimental parameters
2. ANALYTICAL INFORMATION FROM MÖSSBAUER SPECTRA
 - 2.1 Fingerprint method
 - 2.2 Pattern analysis
 - 2.3 Spectrum evaluation
 - 2.4 Databases for analytical Mössbauer spectroscopy
 - 2.4.1 Bibliographical databases
 - 2.4.2 Search systems for Mössbauer data on minerals and geological samples
 - 2.5 Quantitative analysis
3. EXAMPLES FROM APPLICATIONS IN MINERALOGY AND GEOLOGY
 - 3.1 Microenvironments—site determination
 - 3.1.1 Qualitative analysis
 - 3.1.2 Standard and induced patterns as elementary patterns
 - 3.1.3 Standard and induced patterns as superimposed patterns
 - 3.1.4 Patterns with overlapping peaks
 - 3.1.5 Quantitative site analysis
 - 3.1.6 Neighbor effects
 - 3.2 Microenvironment—valence state determination
 - 3.2.1 Isomer shift systematics of microenvironments
 - 3.2.2 Determination of the $\text{Fe}^{2+}/\text{Fe}^{3+}$ ratio
 - 3.3 Microenvironment—characterization of magnetic state
 - 3.3.1 Ferromagnetism
 - 3.3.2 Ferrimagnetism

- 3.3.3 Antiferromagnetism
- 3.3.4 Magnetic relaxation
- 3.3.5 Grain size determination
- 3.4 Transformed pattern—amorphous and poorly crystallized state
- 3.5 Transformed pattern—crystalline state with a multitude of microenvironments
- 3.6 Analysis of meteorites
- 3.7 Phase analysis of rocks
- 4. CONCLUSIONS
- 5. REFERENCES

INTRODUCTION

Mössbauer spectroscopy is a valuable analytical tool in a wide range of sciences including geology and mineralogy. It can be used for studying elements that have a Mössbauer-active isotope like iron, tin, gold, etc., just to name a few. It gives information about the oxidation and magnetic state of such elements and about the short-range crystal chemistry of crystalline and amorphous materials containing Mössbauer-active nuclides. As a specific feature of the method, we emphasize that the various Mössbauer-active nuclides that may be present in the same sample can only be studied consecutively because each Mössbauer spectrum is measured with one particular type of radiation source (e.g., ^{57}Co), which can only be used for the measurement of one particular type of Mössbauer-active nuclide (i.e., ^{57}Fe in the given example).

Iron is the most abundant in geological (and planetological) environments among the elements that can be studied by Mössbauer spectroscopy. The determination of the valence state and the characterization of the coordination polyhedra of iron allows geologists and mineralogists to solve current problems of natural inorganic systems. Such systems may be very different in size, from the local crystal chemistry of individual mineral species to the evolution trends of continents.

In this paper, first we discuss the principles and the analytical practice of Mössbauer spectroscopy in general using a novel terminology, and then we show some examples of how this method can be applied to geology and mineralogy in particular.

1. BASIC PRINCIPLES OF MÖSSBAUER SPECTROSCOPY

Mössbauer spectroscopy [1–5] is based on the recoil-free resonance fluorescence of γ -photons observed with certain atomic nuclei. This method makes it possible to measure nuclear energy levels to an extremely high accuracy (up to 13–15 decimals). Such a precision allows one to measure the slight variation of nuclear energy levels caused by interactions between the electrons and the nucleus. Such interactions reflect changes in the electronic, magnetic, geometric, or defect structure as well as in the lattice vibrations, serving as a basis for a variety of analytical applications.

1.1 Mössbauer parameters

The main Mössbauer parameters are summarized in Fig. 1.

The Mössbauer parameters are presented below in the simplest possible way. For a more detailed interpretation, see the literature [1–15].

The **chemical isomer shift** δ_{C} [8] is a parameter arising from the nuclear energy shift caused by the electric monopole interaction between the nucleus and the (s) electrons that have nonzero density at the site of the nucleus. Thus, the chemical isomer shift is influenced by the oxidation state and by the occupation numbers of electronic orbitals. A simplified formula implying this is as follows:

$$\delta_C = \Delta E_{IS} \frac{c}{E_0} = \alpha \Delta |\Psi(0)|^2 \quad (1)$$

where ΔE_{IS} is the difference between the median transition energies of the absorber (E_A) and the source (E_S) shown in Fig. 1, which is due to the fact that the Mössbauer nucleus is not naked, but sitting in the middle of well-determined atomic species both in the source and in the absorber; c/E_0 is the Doppler conversion factor from energy to speed (see eq. 23a); c is the speed of light in a vacuum; and $\Delta |\Psi(0)|^2$ is the difference between the electron densities at two identical nuclei, one of which is embedded in the source material, while the other in the absorber material*. The factor α comprises several factors including the relative difference between the nuclear radii of the excited state and the ground state for the same nucleus**. For small nuclei (e.g., ^{57}Fe and ^{119}Sn), α can be considered as being independent of the electron density, depending exclusively on the kind of the nucleus in question. Since the electron density may change from compound to compound (or, sometimes, from site to site), the chemical isomer shifts of different absorbers will be different even if they are measured with the same source (which is the usual thing to do).

| Parameter Formula | ^{57}Fe energy level diagram with allowed transition Source (S) Absorber (A) | Schematic representation of absorption vs. relative speed of source and absorber |
|---|--|--|
| Chemical isomer shift $\delta_C \propto \Delta E_{IS} = \beta \Delta \Psi(0) ^2$ | | |
| Second order Doppler shift $\delta_{SOD} \propto \Delta E_{SOD} = -\frac{\langle u^2 \rangle}{2c^2} E_0$ | | |
| Quadrupole splitting $\Delta \propto \Delta E_Q = \frac{1}{2} eQV_{33} \sqrt{1 + \frac{\eta^2}{3}}$ | | |
| Magnetic splitting $\Delta_m \propto \Delta E_m = -g_I \mu_N B$ | | |
| Peak width $W \geq W_0 \propto 2\Gamma = 2 \frac{\hbar \ln 2}{T_{1/2}}$ | | |

Fig. 1 Representation of the main Mössbauer parameters for the $I = 3/2 \rightarrow 1/2$ transition. $E_0 \approx E_\gamma$ is the median transition energy of the naked nucleus, Γ is the natural line width characteristic of both the emission and absorption profile, and W is the peak width. The δ , Δ , and W values have speed unit (mm/s), while E and Γ have energy unit.

*In general, the source is a standard and the absorber is the studied sample.

**Therefore, it is important that the nuclear radius always changes on excitation—otherwise the isomer shift could not be observed at all.

The **second-order Doppler shift** δ_{SOD} is related to the mean square speed $\langle u^2 \rangle$ of lattice vibrations:

$$\delta_{\text{SOD}} = \Delta E_{\text{SOD}} \frac{c}{E_0} = -\frac{\langle u^2 \rangle}{2c^2} E_0 \frac{c}{E_0} = -\frac{\langle u^2 \rangle}{2c} \quad (2)$$

where ΔE_{SOD} is the energy shift shown in Fig. 1. It follows from the above formula that δ_{SOD} decreases with the increase of temperature.

Isomer shifts δ , i.e., the **peak shifts** actually observed in Mössbauer spectra, consist of two terms:

$$\delta = \delta_{\text{C}} + \delta_{\text{SOD}} \quad (3)$$

where the first term is the chemical isomer shift δ_{C} , presented by eq. 1, which does not depend on the temperature, and the second term δ_{SOD} is the second-order Doppler shift [5] discussed above. Since the latter is temperature-dependent (hence, the synonym temperature shift), the whole expression of δ is also temperature-dependent.

The **quadrupole splitting** Δ [9] arises from the splitting of the nuclear energy levels caused by the inhomogeneous electric field of valence electrons and ligands. This interaction is determined by the **nuclear quadrupole moment** (Q) and the components E_{ij} of the **electric field gradient** (EFG) tensor caused by valence electrons and ligands at the nucleus. If the excited state is characterized by nuclear spin quantum number $I = 3/2$ and the ground state by $I = 1/2$ (which is the case with ^{57}Fe and ^{119}Sn), the quadrupole splitting is given by the formula:

$$\Delta = \Delta E_{\text{Q}} \frac{c}{E_0} = \frac{1}{2} eQV_{33} \sqrt{1 + \frac{\eta^2}{3}} \frac{c}{E_0} \quad (4)$$

where e is the elementary charge; ΔE_{Q} is the energy shift shown in Fig. 1; and η is the **asymmetry parameter** calculated from the second derivatives of the electric potential V

$$\eta = \frac{V_{11} - V_{22}}{V_{33}}. \quad (5)$$

Note that the components of the EFG are obtained from the respective potential derivatives as follows:

$$E_{ij} = -V_{ij} \equiv -\frac{\partial^2 V}{\partial x_i \partial x_j}$$

and therefore the V_{ij} s are often referred to (incorrectly) as the components of the EFG tensor. The coordinate axes x_1 , x_2 , and x_3 of the Cartesian system are labeled in such a way that:

$$|V_{33}| \geq |V_{22}| \geq |V_{11}|.$$

For a point charge ez situated at $\mathbf{r} = (x_1, x_2, x_3)$, the V_{ij} components at the nucleus ($r = 0$) are as follows:

$$V_{ij} = ez \frac{3x_i x_j - r^2 \delta_{ij}}{r^3} \quad (6)$$

where δ_{ij} is the Kronecker symbol:

$$\delta_{ij} = \begin{cases} 1 & \text{for } i = j \\ 0 & \text{for } i \neq j \end{cases}.$$

The quadrupole splitting is proportional to the peak separation of the corresponding **quadrupole doublet** (Fig. 1), and so it can be determined easily from the Mössbauer spectrum.

If ligand contribution is predominant in the quadrupole interaction, the individual ligands are usually considered as point charges whose effects are calculated from eq. 6. Summing up that equation, one can prove that the quadrupole splitting is zero for the cases of the highest symmetry in coordination and charge distribution (spherical, “ideal” hexahedral, octahedral, and tetrahedral). However, the often-cited statement that the lower the symmetry, the larger the quadrupole splitting is an oversimplification, which can lead to incorrect conclusions. (For instance, the ligand contribution of the EFG for an octahedral *trans* FeA₂B₄ complex is twice that for the corresponding *cis* configuration although the former one is obviously more symmetrical.)

The quadrupole splitting can also depend on the temperature (see the next section) owing to the temperature-dependent population of valence levels.

The **magnetic splitting** Δ_m [5] observed in Mössbauer spectra arises from the Zeeman splitting of the energy levels of the nucleus provided that a nonzero **magnetic flux density**, B , exists there. The formula of Zeeman splitting is given as follows:

$$\Delta_m = \Delta E_m \frac{c}{E_0} = -g_I \mu_N B \Delta m_I \frac{c}{E_0} \quad (7)$$

where ΔE_m is the energy shift illustrated by Fig. 1 for the $I = 3/2 \rightarrow 1/2$ transition of ^{57}Fe (in the special case of $\Delta m_I = 1$); g_I is a nuclear factor that depends on the nuclear spin I of the nucleus; m_I is the magnetic quantum number; and μ_N is the nuclear magneton. It follows from the above formula that Δ_m has different values for the excited state (e) and for the ground state (g).

The magnetic flux density at the nucleus is proportional to the peak separation of the corresponding **magnetic sextet** (Fig. 2), and so it can be determined very easily from the Mössbauer spectrum.

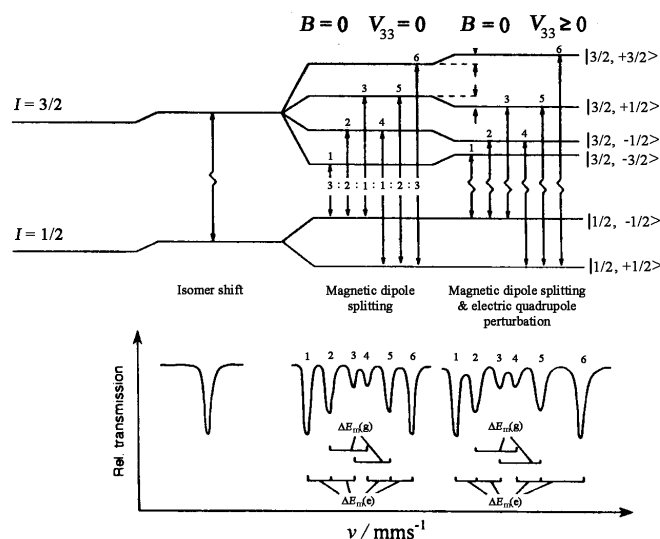


Fig. 2 Magnetic splitting with and without quadrupole interaction for ^{57}Fe [11].*

*The conventional unit of the (components of) isomer shift, quadrupole splitting, magnetic splitting, and peak width is mm/s in Mössbauer spectroscopy. The reason is as follows. When the spectrum is measured (see Fig. 9), the energy of the γ -ray is modulated via the Doppler effect. Since the Doppler speed of the source relative to the absorber is directly available, it is more convenient to scale the abscissa in speed unit than in energy. Note that the Doppler speed and the energy (shift) are in linear relationship with each other according to eq. 23a.

Magnetic splitting is not restricted to materials showing “actual” magnetism like ferromagnetic solids (e.g., α -Fe at room temperature) and ferrimagnetic ones (e.g., magnetite at room temperature). It can also be observed with antiferromagnetic crystals (e.g., with hematite or with MnO) in which the magnetic moments of the different sublattices cancel each other, and thus they are not attracted by a magnet (see Fig. 3). Even paramagnetic materials may produce magnetic splitting if the “flipping” of the unpaired spin is relatively slow for some reason.

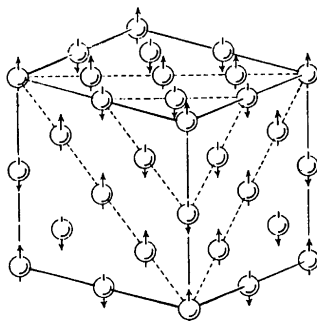


Fig. 3 The antiferromagnetic structure of MnO [16].

The **Mössbauer–Lamb factor** f [7] (also called, erroneously, the Debye–Waller factor) is a measure of the probability of recoil-free resonance fluorescence of γ -photons. It is defined as the number of recoil-free γ events (emission or absorption) divided by the total number of γ events. It can be expressed by the following equation:

$$f = \exp\left(-\frac{4\pi^2\langle r^2 \rangle}{\lambda^2}\right), \quad (8)$$

where λ is the wavelength of the γ -radiation of the Mössbauer transition and $\langle r^2 \rangle$ is the mean-square amplitude of the vibration of the Mössbauer atom “frozen” in the lattice.

The Mössbauer–Lamb factor is one of the coefficients, that determine the Mössbauer peak area A as a function of the concentration of the atomic species which is reflected by that particular spectrum peak (or more generally, by the respective peak pattern discussed later). Since the relationship is monotonic (close to being proportional), the higher the concentration and the Mössbauer–Lamb factor of a given atomic species, the larger its share from the total spectrum area. In the thin-absorber approximation, e.g., for the **peak area** (intensity) A_k of the k^{th} Mössbauer atomic species, we have:

$$A_k \propto f_{a,k} c_{a,k} \quad (9)$$

where $f_{a,k}$ is the Mössbauer–Lamb factor of the k^{th} Mössbauer atomic species in the absorber and $c_{a,k}$ is the concentration of the same species in the absorber. A more general expression for the peak area is given by eq. 32.

The last Mössbauer parameter to be mentioned is the **experimental peak width** W (full width at half the maximum, FWHM) whose dependence on temperature and absorber thickness is discussed in the next section.

1.2 Dependence of the Mössbauer parameters on experimental parameters

As we have just seen, the main **Mössbauer parameters** that can be derived from a Mössbauer spectrum are as follows: Mössbauer–Lamb factor (f), isomer shift (δ), quadrupole splitting (Δ), magnetic

splitting (Δ_m), peak width (W), and the relative area—also called the relative intensity—of the spectrum peaks (A). Sometimes, it is convenient to consider these parameters as the coordinates of the Mössbauer parameter vector \mathbf{P}_M :

$$\mathbf{P}_M = (f, \delta, \Delta, \Delta_m, W, A),$$

where the individual symbols between the parentheses may again represent sets of similar parameters (i.e., vectors). For instance, instead of A we might write \mathbf{A} meaning:

$$\mathbf{A} = (A_1, A_2 \dots),$$

where $A_1, A_2 \dots$ represent the spectral areas of different (sets of) peaks.

The Mössbauer parameters depend on a number of various **experimental parameters** such as the temperature (T), the pressure (p), the external magnetic flux density if any (B_{ext}), the polar angles of the sample relative to the direction of the γ -rays (θ, ϕ), the frequency of high-frequency field (ν), etc.:

$$\mathbf{P}_M = f(\mathbf{P}_{\text{exp}}),$$

where the vector \mathbf{P}_{exp} represents all of the relevant experimental parameters:

$$\mathbf{P}_{\text{exp}} = (T, p, B_{\text{ext}}, \theta, \phi, \nu, c \dots)$$

in which we have also included c denoting the concentration of the Mössbauer species in the sample.

Some of the above-listed experimental parameters have **standard values**. For instance, $T_0 = 293$ K (room temperature, RT), $p_0 = 1$ bar (~atmospheric pressure), $B_{\text{ext},0} = 0$ T (no external magnetic field applied), etc. The measuring conditions specified by such values are called **standard conditions**.

The **temperature dependence** of Mössbauer parameters can be measured relatively easily. It also turns out very useful in qualitative analysis. The same sample is measured at different temperatures, because the temperature dependence is often different for the different spectrum components, and, therefore, this may help distinguish between species whose “fingerprints” are similar under standard conditions (i.e., at room temperature in the given instance) but different at lower or higher temperatures.

- *Isomer shift*. The temperature dependence of the isomer shift (see Fig. 4) is determined by that of the second order Doppler shift implied by eq. 2.

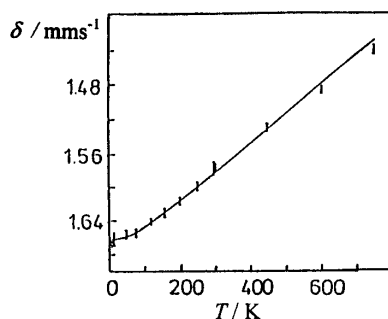


Fig. 4 Temperature dependence of the isomer shift of ^{119}Sn in $\text{V}_3\text{Ga}_{0.1}\text{Sn}_{0.9}$ [8].

- *Quadrupole splitting*. The temperature dependence of the quadrupole splitting comes from the temperature-dependent population of the different valence levels, provided that the valence contribution to the electric field gradient is not negligible. The temperature dependence of quadrupole splitting is illustrated by Fig. 5 for $\text{Cd}_3[\text{Fe}(\text{CN})_6]_2$.

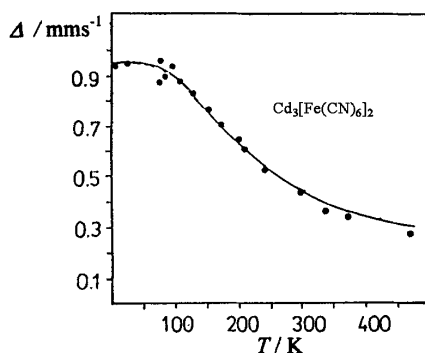


Fig. 5 Temperature dependence of the quadrupole splitting of ^{57}Fe in $\text{Cd}_3[\text{Fe}(\text{CN})_6]_2$ [15; p. 78].

• *Mössbauer–Lamb factor.* The temperature dependence of the Mössbauer–Lamb factor (see Fig. 6) can be calculated from the Debye model [15] of solids:

$$f(T) = \exp \left\{ -\frac{3E_R}{2k\Theta_D} \left(1 + 4 \int_0^{\frac{\Theta_D}{T}} \frac{x}{e^x - 1} dx \left(\frac{T}{\Theta_D} \right)^2 \right) \right\}, \quad (10)$$

where E_R is the recoil energy of the nucleus determined by the nuclear mass m_N and γ -energy E_γ :

$$E_R = \frac{E_\gamma}{2m_N c^2}$$

k is Boltzmann's constant, Θ_D is the characteristic Debye temperature:

$$\Theta_D = \frac{\hbar\omega_D}{k} \quad (11)$$

and ω_D is the minimum of the angular frequency of phonons.

For $T \ll \Theta_D$ we get from the Debye model of solids [15]:

$$f(T) = \exp \left\{ -\frac{E_R}{k\Theta_D} \left(\frac{3}{2} + \frac{\pi^2 T^2}{\Theta_D^2} \right) \right\}. \quad (12)$$

• *Magnetic splitting.* The temperature dependence of the magnetic splitting itself depends on the nature of the magnetic interaction in the investigated material.

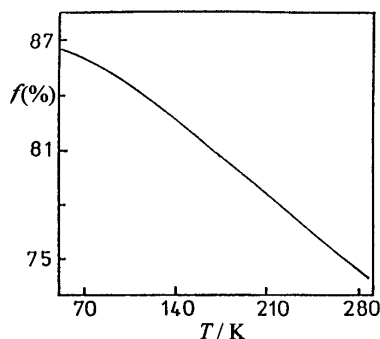


Fig. 6 Temperature dependence of the Mössbauer–Lamb factor of ^{57}Fe .

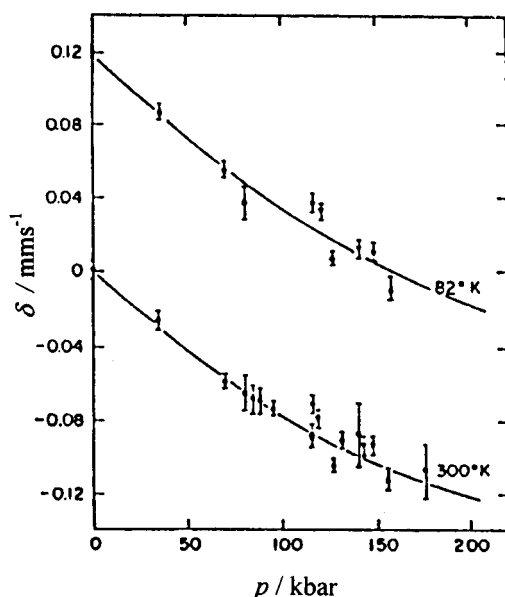


Fig. 7 Pressure dependence of the isomer shift of ^{57}Fe in $\alpha\text{-Fe}$ [8].

For simple **ferromagnetic** interaction, e.g., when the Bloch-law [16] is valid for the field, we get

$$\frac{\Delta E_m(T)}{\Delta E_m(0\text{ K})} = 1 - C T^{3/2} \quad (13)$$

where C is a coefficient.

In the case of some **paramagnetic** materials exhibiting magnetically split Mössbauer spectra, the magnetic splitting is due to the paramagnetic spin relaxation time τ_{SR} being relatively high in comparison with the **mean life** ($\tau = T_{1/2}/\ln 2$) of the excited state of the Mössbauer nucleus. In this case, temperature dependence is governed by that of the spin-lattice relaxation of the material [15,17].

• *Peak width.* The temperature dependence of the peak width W caused by the diffusive motion of resonant nuclei can be expressed either by the formula

$$\frac{\Delta W}{W} = \exp\left(-\frac{E^*}{kT}\right)$$

or by

$$\Delta W = \frac{2c\hbar}{E_0\tau_0} \left[1 - \int e^{ikr} h(r) dr\right], \quad (14)$$

where E^* is the activation energy, k is the wave vector of the γ -photon, $h(r)$ is the probability density of finding an atom after one jump at point r relative to the origin of the jump, and τ_0^{-1} is the jump frequency.

The **pressure dependence** of Mössbauer parameters follows from that of the physical quantities that determine the values of those parameters. The pressure dependence of the isomer shift [8], as illustrated by Fig. 7. (Pressure dependence may turn out very important for the experimental modeling of the upper and lower mantle conditions.)

The **external magnetic field dependence** of Mössbauer parameters can be very important, because—by choosing an appropriate external magnetic flux density—one often gets a better resolved spectrum.

By applying an external magnetic field, one can produce sources of polarized ^{57}Fe γ -rays. (^{57}Fe is the most frequently studied Mössbauer nuclide.) This can be done, e.g., by embedding the ^{57}Co parent nuclide in a ferromagnetic host (e.g., in α -Fe) and by magnetically saturating the host material with an appropriate external field. Such a source will emit six lines (instead of just one) which, when overlapping with a simple six-line absorber hyperfine pattern, will lead to 36 (i.e., 6×6) possible absorption peaks (instead of just 6).

The *effective magnetic flux density* B measured at the nucleus consists of two terms:

$$B = B_{\text{ext}} + B_{\text{int}} \quad (15)$$

where B_{ext} is the external magnetic flux density and B_{int} is the *internal magnetic flux density* which, again, consists of a number of components of different origin [17].

The use of external magnetic field makes it possible to determine the sign of the quadrupole splitting from the induced magnetic pattern (see Fig. 2) in the case of ^{57}Fe and ^{119}Sn spectroscopy of non-magnetic materials.

The effect of external magnetic field on the magnetic splitting of magnetic materials depends on the nature of magnetic coupling (i.e., whether the material is ferromagnetic, ferrimagnetic, or antiferromagnetic) [5].

Radio-frequency electromagnetic radiation can have two kinds of effect on the Mössbauer spectrum [18]. It can collapse the Mössbauer pattern, but it can also produce side bands in the spectrum on the basis of which a better identification of the atomic species can sometimes be done.

The **angular dependence of peak areas** is connected with the angular dependence of the transition probabilities of the different nuclear transitions.

• *Magnetic sextets.* The angular dependence of the relative peak areas of a magnetic sextet appearing in ^{57}Fe or ^{119}Sn spectra (both representing the $I = 3/2 \rightarrow 1/2$ nuclear spin transition) is given by the following expressions

$$A_1(\theta) = A_6(\theta) = \frac{3}{16}(1 + \cos^2 \theta) \quad (16)$$

$$A_2(\theta) = A_5(\theta) = \frac{4}{16}(1 - \cos^2 \theta) \quad (17)$$

$$A_3(\theta) = A_4(\theta) = \frac{1}{3}A_1(\theta) = \frac{1}{3}A_6(\theta) = \frac{1}{16}(1 + \cos^2 \theta) \quad (18)$$

where θ is the angle between the respective directions of the γ -ray and the effective magnetic flux density; and the area subscripts refer to the peak numbers of the sextet. (Above, the peak areas are normed so that their sum yields 1 for a complete six-peak pattern.)

In the case of ferromagnetic materials, the direction of the effective magnetic flux density \mathbf{B} can be manipulated by an external field \mathbf{B}_{ext} .

If the direction of the effective magnetic field changes from point to point in a sample so that each direction has the same occurrence, then the relative peak areas (intensities) of the resultant sextet will average out to:

$$A_1:A_2:A_3:A_4:A_5:A_6 = 3:2:1:1:2:3, \quad (19)$$

which is the typical case for antiferromagnetic powder samples without texture. Bulk ferromagnetic materials (e.g., a not too thin piece of α -iron) also have such a tendency, because the magnetic moments of their domains point at random directions.

• *Quadrupole doublets.* In the case of a quadrupole doublet, the relative areas (intensities) of the doublet peaks [11], representing the $m_I = \pm 3/2 \rightarrow \pm 1/2$ and the $m_I = \pm 1/2 \rightarrow \pm 1/2$ transition, respectively, will be

$$A_{\pm\frac{3}{2} \rightarrow \pm\frac{1}{2}}(\theta) = \frac{3}{8}(1 + \cos^2 \theta) \quad (20)$$

$$A_{\pm\frac{1}{2} \rightarrow \pm\frac{1}{2}}(\theta) = \frac{3}{8}\left(\frac{5}{3} - \cos^2 \theta\right) \quad (21)$$

where θ is the angle between the respective directions of the γ -ray and the main axis of the EFG at the nucleus. (The peak areas are normed again so that their sum yields 1 for a complete two-peak pattern.)

In a well-mixed powder sample, where there is a random distribution of electric field gradients, we expect a symmetrical doublet having equal peak areas:

$$A_{\pm\frac{3}{2} \rightarrow \pm\frac{1}{2}} : A_{\pm\frac{1}{2} \rightarrow \pm\frac{1}{2}} = 1 : 1$$

The deviation from the above symmetry is generally an indication of the powder sample being textured. Another possible reason for asymmetry can be the so-called Goldanskii–Karyagin effect, which is caused by the (rare) anisotropy of the Mössbauer–Lamb factor.

The dependence of the experimental peak width (W) on the **absorber thickness** for Lorentzian peaks is given [15] by the following equation:

$$W = \frac{c}{E_0} \Gamma \tau_a \frac{\exp\left(-\frac{\tau_a}{2}\right) I_0\left(-\frac{\tau_a}{2}\right) + I_1\left(-\frac{\tau_a}{2}\right)}{1 - \exp\left(-\frac{\tau_a}{2}\right) I_0\left(-\frac{\tau_a}{2}\right)} \quad (22)$$

where Γ is the natural line width of the given Mössbauer transition, I_0 and I_1 denote modified Bessel functions of the first kind (also referred to as having imaginary argument) and τ_a is the effective thickness of the absorber (which is proportional to the actual thickness d_a measured in mg/cm^2). As to the exact definition of the effective thickness, see eq. 31. Absorber thickness can also be optimized as regards the time necessary to measure a satisfactory spectrum [19].

Figure 8 shows the *peak area*, *peak height*, and *peak width* as the function of effective thickness.

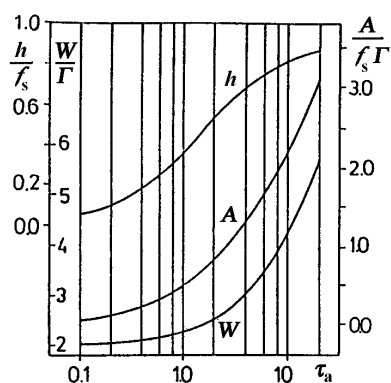


Fig. 8 Dependence of peak area A , peak height h , and peak width W on the effective thickness of the absorber (τ_a) [20]. Γ is the natural line width, and f_s is the Mössbauer–Lamb factor of the source.

The dependence of Mössbauer parameters on **geometric arrangements** is mainly due to the cosine smearing of the velocity v (Fig. 9). Since the Doppler energy shift ΔE_γ is given by

$$\Delta E_\gamma = E_\gamma \frac{v}{c} \cos \theta, \quad (23)$$

(where E_γ is the energy of the emitted γ -photon), a smearing effect can always be observed on the experimental peak shape, peak width, and isomer shift [11], even under “ideal” conditions when we use an anisotropic point source and a circular absorber placed coaxially as illustrated by Fig. 9. (Above, θ is the angle between the γ -ray and the direction of motion of the source or the absorber, whichever is moved.)

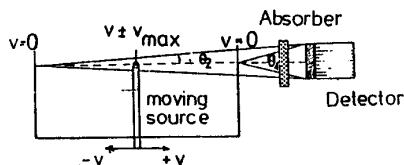


Fig. 9 The origin of cosine effect [11]. In the figure, v is the speed of the source relative to the absorber.

In the axial case (when the angle θ is zero), eq. 23 delivers the usual **conversion factor** between Doppler speed and energy shift used in eqs. 1, 2, 4, and 7:

$$v = \Delta E_\gamma \frac{c}{E_\gamma} \approx \Delta E_\gamma \frac{c}{E_0} \quad (23a)$$

2. ANALYTICAL INFORMATION FROM MÖSSBAUER SPECTRA

2.1 Fingerprint method

As with other analytical techniques, the fingerprint method is one of the most powerful tools of qualitative analysis in Mössbauer spectroscopy.

In general, the fingerprint method operates with **patterns** (“fingerprints”) characteristic of different phases, compounds, crystallographic sites, etc., which we will refer to as **physicochemical entities** for brevity. The correspondence between individual patterns and such entities is determined by the nature of interactions serving as a basis for the analytical method.

In order to understand this correspondence in the case of Mössbauer analysis, let us first discuss the question of what physicochemical entities are reflected by a simple Mössbauer pattern [20].

As mentioned in the previous section, the Mössbauer spectrum reflects the electric and magnetic interactions between the Mössbauer-active nucleus and its environment. Such interactions are commonly called **hyperfine interactions**. Since the hyperfine interactions are determined principally by the electron density and the inhomogeneous electric field as well as by the effective magnetic flux density at the nucleus, Mössbauer spectrum patterns differ from site to site where these physical quantities are different. Thus, a single-phase material may be characterized by a complex Mössbauer spectrum superimposed from a number of simple Mössbauer patterns belonging to resonant atoms experiencing different hyperfine interactions.

The **microenvironment** is a convenient term for the classification of local environments surrounding Mössbauer atoms. The local environments of two Mössbauer atoms represent the same microenvironment if those Mössbauer atoms experience the same hyperfine interaction there. By this definition, a simple Mössbauer pattern is always associated with a microenvironment characteristic of one particular family of Mössbauer nuclei in the studied sample. For brevity, such a family of like Mössbauer nuclei will be referred to as a **Mössbauer species**.

2.2 Pattern analysis

The basic task of the analysis is to identify the individual Mössbauer species from the corresponding patterns present in the spectrum. Ideally, this can be done if there is an exact correspondence between them.

Unfortunately, such a one-to-one correspondence between Mössbauer species and individual patterns may be nonexistent under the given conditions (i.e., for that particular set of experimental parameters at which the Mössbauer spectrum was recorded). However, when the whole range of the possible conditions is considered, we may find points in the space of experimental parameters at which only one pattern is associated with one species and vice versa, and thus we can get round the problem of ambiguity. We can also do simultaneous evaluation of a whole series of Mössbauer spectra taken from the same sample under different conditions. Such a **serial evaluation** is a very effective tool, because the known dependences of the Mössbauer parameters (e.g., isomer shift) on the externally set experimental parameters (e.g., temperature) can be used as constraints for the serial fit.

From the analytical point of view, we can classify **Mössbauer patterns** in the following way.

According to **experimental conditions**, we have:

- standard patterns,
- induced patterns.

According to **complexity**, we have:

- elementary patterns,
- superimposed patterns.

According to **mathematical processing**, we have:

- natural patterns,
- transformed patterns.

A Mössbauer spectrum can be a simple spectrum (elementary pattern) reflecting only a unique microenvironment/Mössbauer species or a complex spectrum (superimposed pattern), which consists of a number of subspectra.

The **standard pattern** is associated with a Mössbauer spectrum obtained at a standard set of experimental parameters. In most laboratories, for example, measurements performed at room temperature, under atmospheric pressure and without external magnetic field are considered as standard. The **induced pattern**, however, is obtained under conditions other than standard (e.g., measurements performed in a cryostat or a furnace, or in the field of a magnet, etc.). In this case, the differences between the induced and standard patterns can give important contribution to the analysis*.

The **elementary pattern** is associated with one type of microenvironment/Mössbauer species. The **superimposed pattern** is the superposition of elementary patterns.

*We call it an induced pattern because on the one hand it is “induced” by changing the external conditions and on the other hand because a split pattern can be “induced” in the spectrum by applying external fields or by lowering the temperature (see previous section).

The **transformed pattern** is obtained from the measured Mössbauer spectrum (i.e., from the **natural pattern**) by mathematical transformation (e.g., by Fourier transformation). For instance, the magnetic hyperfine field (i.e., effective magnetic flux density) distribution or the quadrupole splitting distribution are considered transformed patterns*. The transformed pattern may give a better resolution for the analysis.

Figures 10a and 10b illustrate the relation between different types of patterns and the object of the analysis as well as the most common strategy followed when doing qualitative analysis by Mössbauer spectroscopy. Generally, the Mössbauer spectrum of a multicomponent/multiphase material is a superposition of superimposed patterns. This is so because each compound/phase can have different crystallographic sites, each site represented by a different pattern. Note that even a single crystallo-

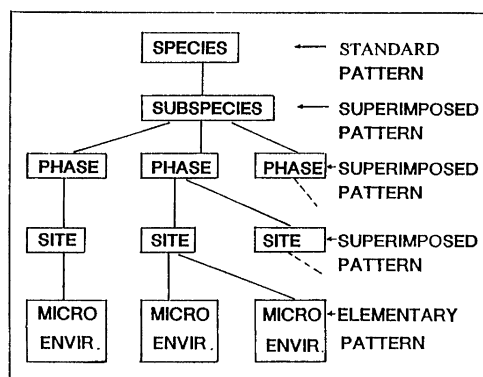


Fig. 10a Relation between different types of patterns and the object of analysis [20].

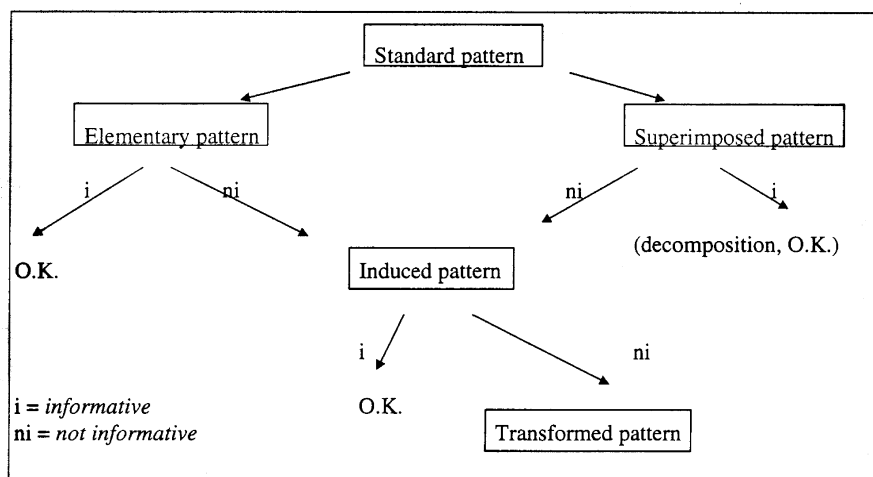


Fig. 10b Simplified strategy of qualitative analysis by Mössbauer spectroscopy.

*The concept of the *transformed pattern* is based on practical considerations. Stripped spectra, of course, are *transformed spectra*. However, when stripping actually affects the rest of the elementary patterns (i.e., when the elementary patterns themselves are "transformed" by the stripping process), that is a clear indication of something going wrong with the evaluation. The role of the mathematical transformations that we consider is to transform the individual patterns so that they can be better resolved than the original ones. This can help even when the conventional stripping technique is not able to solve the problems, e.g., in the case of nanocrystalline or amorphous materials.

graphic site may represent more than one microenvironment owing to variations in the hyperfine interactions (e.g., different electronic and spin density, defect arrangement, etc.).

In order to give an example, let us consider an omphacite sample in which Fe^{2+} and Fe^{3+} ions are present in the M1 site. The standard pattern (^{57}Fe Mössbauer spectrum) of the sample is a complex spectrum that is the sum of subspectra (Fig. 11). The subspectra of the Fe^{2+} and Fe^{3+} ions are also superimposed from elementary patterns owing to the effect of different neighboring cations.

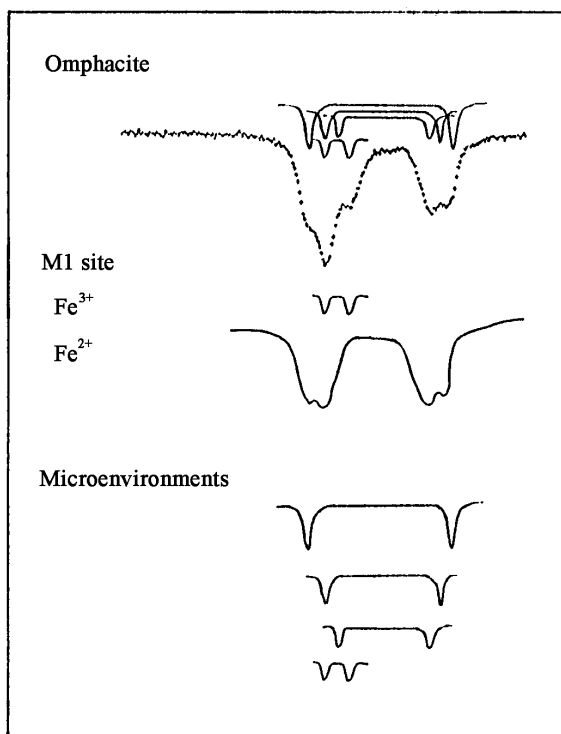


Fig. 11 The standard pattern of omphacite [21]. A more detailed discussion of omphacite will be given in Section 3.1 in connection with Fig. 23 and Table 1.

Very often, when the characteristic subspectra of components are well distinguishable in the standard spectrum, the qualitative analysis can be performed without the need for measuring further non-standard spectra (induced patterns). In general, however, the subspectra (elementary patterns) overlap each other in the standard spectrum. When the exact decomposition of the spectrum becomes ambiguous, it is still possible to get further analytical information from an induced pattern (e.g., via serial evaluations).

For example, the standard room-temperature patterns of akageneite ($\beta\text{-FeOOH}$) and lepidocrocite ($\gamma\text{-FeOOH}$) are paramagnetic doublets with similar parameters. So they cannot be easily differentiated. However, the induced patterns of $\beta\text{-FeOOH}$ taken below the magnetic transition temperature (Fig. 12) [20] reflect magnetically split subspectra (sextets). Now, by the help of the induced pattern, the analytical problem can be solved more easily.

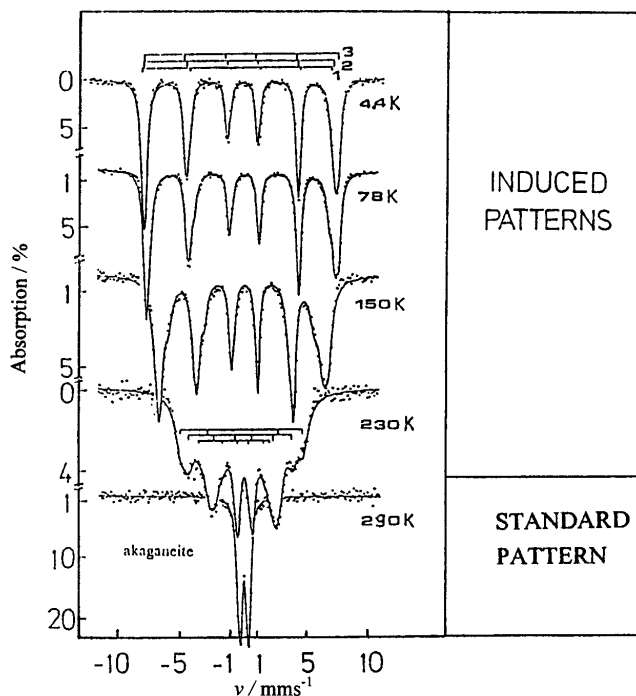


Fig. 12 The induced patterns of akaganeite [20] carry much more information for the analysis than the standard one.

In some cases, the natural pattern consists of hundreds of elementary patterns. This is the typical situation with poorly crystallized and amorphous systems. The transformed pattern (Fig. 13) can help get more information about the short-range ordering (by characterizing some of the most probable arrangements), thus it can enhance the analytical applicability.

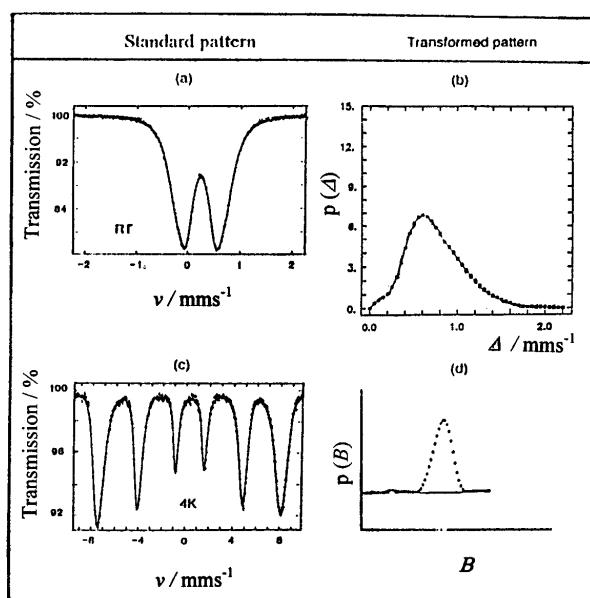


Fig.13 The transformed patterns (graphs on the right side) of poorly crystallized ferrihydrite.

2.3 Spectrum evaluation

Mössbauer spectra encountered in the practice can be fairly complex. In order to get any analytical information from such a spectrum, it has to be decomposed to elementary patterns first, or it must be converted to a transformed pattern.

In the practice of Mössbauer spectroscopy, the **Mössbauer parameters** are determined by the computer evaluation of spectra. The Mössbauer parameters are derived from the **peak parameters** (base line parameters, peak position, peak width, peak area/height) via the fitting process. Alternatively, the distributions of certain Mössbauer parameters [22,23] or the joint distributions of several Mössbauer parameters [27] are directly derived from the spectrum.

For the regular spectrum evaluation, an *a priori* knowledge of both the peak-shape function and the connection between the Mössbauer parameters and the peak parameters is necessary.

The Mössbauer peak shape used in the fitting process depends on the sample and on the computing facilities that are available for the spectroscopist. The fitting programs used nowadays usually run on personal computers. There is a recent trend of developing user-friendly and versatile programs for this purpose [24].

The most precise way of fitting is based on the computation of the transmission integral given by eq. 30.

Very often, however, the simple Lorentzian peak shape is considered:

$$L(u) = \frac{1}{\pi} \frac{W}{2} \frac{A}{(u - u_0)^2 + \left(\frac{W}{2}\right)^2} = \left(\frac{W}{2}\right)^2 \frac{h}{(u - u_0)^2 + \left(\frac{W}{2}\right)^2} \quad (24)$$

where u_0 is the position (in mm/s), W is the width, A is the area (intensity), and h is the height of the peak. This can be a good approximation, if the absorber is sufficiently thin (the effective thickness τ_a should be less than 1) and if the number of overlapping peaks is not very large (less than 10).

For the analysis of materials whose spectra consist of a large number of overlapping peaks (e.g., amorphous metals), the product (or rather the convolution) of Lorentzian and Gaussian curves (Voigt function) is used to fit the peaks [25].

The spectrum fitting is done by the least-squares method by using an appropriate model function S (e.g., a linear combination of Lorentzians). In this procedure, the sum

$$\chi^2 = \sum_{i=1}^k \frac{1}{N_i} \left[N_i - S(i; \mathbf{P}_{\text{peak}}) \right]^2 \quad (25)$$

is minimized, where N_i is the number of counts stored in the i^{th} channel; k is the total number of channels. The model function S is determined by the vector \mathbf{P}_{peak} of the peak parameters that is set up from the individual parameter vectors of the baseline (\mathbf{p}_0) and the peaks ($\mathbf{p}_1, \mathbf{p}_2, \dots, \mathbf{p}_n$):

$$\mathbf{P}_{\text{peak}} = (\mathbf{p}_0, \mathbf{p}_1, \mathbf{p}_2, \dots, \mathbf{p}_n). \quad (26)$$

Each parameter vector \mathbf{p}_j itself represents a set of three parameters characterizing the position, width and area/height of the j^{th} peak out of the n .

In the thin-absorber approximation, an inhomogeneous linear transformation is used to make connection between the vector of the Mössbauer parameters \mathbf{P}_M (set up from isomer shifts, quadrupole splittings, magnetic splittings, etc.) and the vector of the peak parameters \mathbf{P}_{peak} :

$$\mathbf{P}_M^T = \mathbf{T} \mathbf{P}_{\text{peak}}^T + \mathbf{C}^T \quad (27)$$

where the constrains are determined by the elements of the transformation matrix \mathbf{T} and the constant vector \mathbf{C} . (The superscript T indicates that we have column vectors in the formula.)

The a priori knowledge of the matrix T and the vector C is normally an essential condition of spectrum evaluation*. From the point of view of analytical applications, the a priori determination of the T matrix is of fundamental importance. Namely, this transformation enables the experimenter to specify a set of peaks as a pattern representing one particular Mössbauer species in the sample.

In other words, in order to be able to evaluate a spectrum, we must have some kind of a hypothesis about the relations among the spectral peaks. Then the validity of this hypothesis can be verified by the fitting itself. The hypothesis must be based upon our previous knowledge about the material under study. Looking at the spectrum, we have to determine the total number of spectral peaks first. This is not so easy in the case of overlapping subspectra. The incorrectly chosen number of peaks renders the analysis itself incorrect.

If the available information is insufficient, a systematic successive trial can lead to a possible set of peaks composed from a minimum number of peaks still giving a satisfactory fit**. However, in such a case, the correct grouping of the peaks can rarely be obtained from the standard pattern alone. It is necessary to compare the results with the evaluations of nonstandard spectra (induced patterns) and with the spectra of etalons as well as with theoretical considerations.

Any preliminary information about the sample (history, results obtained with other methods) can help identify prospective Mössbauer species whose patterns can be considered when setting up the T matrix. Such patterns can sometimes be recognized by visual inspection. If this is the case, the **stripping technique** can help further explore the components present. This technique involves that the recognized and appropriately scaled subspectrum (or a reference spectrum) is subtracted from the recorded spectrum. Then a new component can be more easily discovered in the residuum spectrum than in the original one. The stripping of the spectrum is continued by the subtraction of the newly found component. The iteration procedure is continued until the residuals become satisfactorily small. Finally, every spectral component can be assigned.

The assignment of the subspectrum to one particular Mössbauer species is based on the comparison of the derived pattern with a reference spectrum. The **reference spectrum** can be obtained by measuring an etalon material or from the data published in the literature. In some cases, the reference spectrum can be constructed theoretically (computer simulation).

A special way of spectrum evaluation is done by obtaining and analyzing transformed patterns. For a thin absorber, the spectrum shape $S(u)$ can be described as the convolution of a density function $f(u)$ with a Lorentzian function $L(u)$:

$$S(u) = \int_{-\infty}^{+\infty} f(v)L(u-v)dv. \quad (28)$$

One of the methods [22–27] for obtaining the distribution of effective magnetic flux density or quadrupole splitting is the **Window method** [22] that uses a Fourier technique. For instance, the *distribution of the effective magnetic flux density* (also called *hyperfine field distribution*)

$$p(B) = \sum_i^N a_i \left[\cos \frac{B_i - B_{\min}}{B_{\max} - B_{\min}} - (-1)^i \right] \quad (29)$$

can be obtained by fitting the spectrum (B_{\min} and B_{\max} are the minimum and maximum values of the effective magnetic flux density). Although it is very time-consuming to get the correct distribution func-

*Sometimes it would be nice, however, to be able to fit the elements of the transformation matrix itself. Asymmetric doublets appearing in the spectra of textured samples, for example, could then be handled more easily, because the asymmetries could be fitted together using reasonable constraints.

**A similar approach is suggested whenever the problem actually calls for the fitting of the elements of the transformation matrix itself (which is impossible directly). This strategy is recommended, for example, in the case of textured samples mentioned in the previous footnote.

tion, this method has a very important advantage, since no a priori knowledge is required to get the transformed pattern.

Rancourt [27] has stressed the advantages of operating with the joint normal distribution of all the Mössbauer parameters characterizing the same physicochemical entity. The **Rancourt method** eliminates the necessity of assuming a deterministic (e.g., linear) dependence of the studied parameter (e.g., the effective magnetic flux density in the case of the Window method) on another parameter (e.g., the isomer shift for the same method). Instead, it reveals their stochastic relationship by providing their local correlation typical of a given site, etc.

2.4 Databases for analytical Mössbauer spectroscopy

2.4.1 Bibliographical databases

There are several data collections giving assistance for searching the literature for *Mössbauer reference data* of a given mineral or compound. The most important and most comprehensive source is the Mössbauer Information System (MIS) of the Mössbauer Effect Data Center (MEDC) at the University of North Carolina at Ashville, NC, USA, a scientific center collecting Mössbauer data since the discovery of the Mössbauer effect (1958). The MIS contains about 35 000 bibliographic references. The majority of these data represent standard patterns.

The new entries of MIS are regularly published in the volumes of Mössbauer Effect Reference and Data Journal (MERDJ) [28]. Currently, one volume of MERDJ consists of 10 issues and a special Index issue, and covers a year of literature search. This journal lists all the published Mössbauer data according to the Mössbauer transitions.

From time to time, MEDC compiles and publishes special sub-databases of MIS. The latter, called MÖSSBAUER MICROS, running in a personal computer environment, offers the references and qualitative information about the Mössbauer parameters found in the literature [28,29].

2.4.2 Search systems for Mössbauer data on minerals and geological samples

It is not customary yet to set up search systems that are primarily based on measured Mössbauer data and not on a priori other knowledge (e.g., chemical composition, mineral name, etc.) concerning the sample.

There are two factors that exclude the possibility of a general mineral identification system based on Mössbauer data only, namely:

- Mössbauer spectroscopy is mainly sensitive to the short-range order and not to the long-range order,
- only a restricted number of elements have Mössbauer-active isotopes.

On the other hand, the large number of iron, antimony, gold, etc., minerals and those minerals having no Mössbauer-active elements in their formula but containing iron, europium, gold, tin, etc., as minor or trace elements still justifies the creation of Mössbauer mineral databases of limited extension.

Such a search system for minerals has been reported by de Souza, Jr. et al. [30]. Their software called Mössbauer Effect Assistant (MEA) is based on a data bank of 478 iron-containing minerals reported in the literature between 1958 and 1994. The program uses a Learning Vector Quantization (LVQ) Artificial Neural Network (ANN), which is linked to the Mössbauer data bank containing the Mössbauer parameters (isomer shift, quadrupole splitting, effective magnetic flux density), the source/matrix specification, the temperature of the absorber, and the references of the published minerals. The program identifies the mineral under study and/or its crystal structure when fed with the experimental Mössbauer parameters. It can also list the references of the literature that are stored in the data bank when feeding the name of a substance or the author of a publication. The MEA runs in Microsoft Windows environment.

It seems to be desirable, however, to have a *general search system for Mössbauer data* that could play a similar role in Mössbauer spectroscopy as the JCPDS system (Hanawalt-system) in X-ray diffractometry. The terminology suggested in subsections 2.1 and 2.2 can help systematize the Mössbauer data for the identification of individual physical or chemical species from the corresponding patterns present in the spectrum [31].

2.5 Quantitative analysis

In Mössbauer spectroscopy, as in other spectroscopic methods, quantitative analysis is based upon the determination of peak areas.

In the case of an ideally thin source and a not-so-ideally thin absorber (with Mössbauer–Lamb factors f_s and f_a , respectively), the peak shape can differ from the simple Lorentzian. The probability of a resonance photon's passing through the absorber can be given as

$$T(u) = \exp(-\mu_a d_a) \left[(1-f_s) + \frac{f_s \Gamma}{2\pi} \int_{-\infty}^{+\infty} \frac{1}{(E-E_0(1+u/c))^2 + (\Gamma/2)^2} \exp\left(-\tau_a \frac{(\Gamma/2)^2}{(E-E_0)^2 + (\Gamma/2)^2}\right) dE \right] \quad (30)$$

which is known as the **transmission integral**. Above, u is the speed of the source relative to the absorber at the moment of photon emission, Γ is the natural line width of the Mössbauer transition as determined by the relation $\Gamma T_{1/2} = \hbar \ln 2$ (where $T_{1/2}$ is the half-life of the excited state of the Mössbauer nucleus), μ_a is the electronic absorption coefficient, and τ_a is the effective thickness of the absorber.

The **effective thickness** τ_a of the absorber is proportional both to the number of Mössbauer atoms in the unit volume of the absorber (v_a), and to the absorber thickness (d_a):

$$\tau_a = \sigma_0 d_a f_a v_a \quad (31)$$

where σ_0 is the maximum of the resonant cross-section.

The area (intensity) A_T of the transmission peak can be expressed as

$$A_T = \int_{-\infty}^{+\infty} \frac{T(\infty) - T(u)}{T(\infty)} du = \frac{\pi \Gamma f_s}{2} \tau_a \exp\left(-\frac{\tau_a}{2}\right) \left[I_0\left(\frac{\tau_a}{2}\right) + I_1\left(\frac{\tau_a}{2}\right) \right] \quad (32)$$

where I_0 and I_1 denote modified Bessel functions of the first kind, which first appeared in eq. 22.

The contour of the normalized Mössbauer spectrum can be expressed by the transmission integral:

$$S(u) = (1-b) \frac{T(\infty) - T(u)}{T(\infty)}, \quad (33)$$

where b is the background fraction of photons behind the absorber (i.e., the fraction of photons that do not originate from the Mössbauer transition). The area of the normalized spectrum is:

$$A_S = (1-b)A_T. \quad (34)$$

Implicitly, the above equation defines the peak area as an increasing function of the effective thickness (the latter being proportional to the concentration of the resonant atoms), thus making it the single most important parameter of quantitative analysis. The number of resonant atoms in the unit volume of the absorber (v_a) is calculated from the area by a computer.

In the **thin-absorber approximation** ($\tau_a < 0.1$), it can be shown that the *peak area* is proportional to the Mössbauer atom concentration:

$$A \approx k \tau_a = k \sigma_0 d_a f_a v_a = k \sigma_0 d_a f_a n_a a \quad (35)$$

where a is the fractional abundance of the Mössbauer isotope (e.g., that of ^{57}Fe in natural iron) and n_a is the number of atoms of the studied Mössbauer element (e.g., iron) per unit volume of the absorber. The constant k includes other constants and parameters involving the background and matrix effects. This equation also shows that the area of a Mössbauer peak is proportional to the number of Mössbauer atoms in a thin sample.

Although the above approximation is widely used whenever Mössbauer spectroscopy serves as a tool of quantitative analysis, the relative error committed is about 5 % even at $\tau_a = 0.1$ [15].

For the determination of the concentration n_a all the parameters in eq. 35 are necessary to know. However, in most cases, the exact values of the Mössbauer–Lamb factor f_a and the constant k are unknown. In such a case, calibration graphs are drawn by measuring the spectra of a series of analogous samples having different known concentrations. For the same purpose, internal etalons can also be used.

The relative concentrations of the individual Mössbauer species can be determined more accurately by the Mössbauer method than the respective absolute concentrations. Consequently, most applications aim the determination of relative concentrations. There are, however, such cases, when the relative concentrations of the subspecies of the resonant nuclide yield as a spinoff the absolute concentration of another nonresonant element.

3. EXAMPLES FROM APPLICATIONS IN MINERALOGY AND GEOLOGY

The examples presented in this section are selected from the mineralogical and geological applications of Mössbauer spectroscopy for the following reasons:

- Mössbauer spectroscopy can be applied to perform qualitative and quantitative analysis of Mössbauer-element-bearing mineral phases occurring not only in crystalline, but also in amorphous or poorly crystallized state.
- Mössbauer spectroscopy has become a standard tool of earth scientists during the last decades.
- Mineralogy is one of the widest analytical application areas of Mössbauer spectroscopy.
- The Mössbauer patterns of minerals are usually complex, and therefore pattern analysis is needed. The spectral envelope is generally not sufficient for analytical identification.
- Microenvironments bear important information. Site assignment of Mössbauer subspectra has already been performed in many cases, however, our terminology gives a guideline for using pattern analysis to future problems to solve.
- This field serves with lots of examples for what types of errors should be avoided when doing analytical Mössbauer spectroscopy (see some of the most important points of our criticism below).

In most mineralogical applications of Mössbauer spectroscopy, the spectra of the minerals are only recorded at room temperature. Moreover, very often, the reader can only assume that the reported results refer to room temperature, because the authors “forget” to mention the values of the externally set experimental parameters at which the spectrum has been taken.

Spectrum evaluation often seems to be rather arbitrary and subjective. It is not uncommon that only the average parameters of the spectral envelope are reported. The spectra are usually decomposed to a minimum number of subspectra resulting in a satisfactory fit by the least-square fitting of Lorentzians. Only individual spectra are evaluated when a serial evaluation of several spectra would be the solution. This simultaneous evaluation of spectra, recorded under different external conditions, of the same sample is practically nonexistent in this field. The use of distribution-extracting methods for the spectrum evaluation is also very rare.

Consequently, the Mössbauer parameters of the same mineral show very large variation in the literature, much larger than it could be attributed to the actual difference between the investigated samples. If one wants to use the mineral handbook [29] to find reference parameters in order to analyze a newly measured spectrum of a mineral, he/she will meet the problem of how to select data, because so

much different (and in many cases contradictory) parameters exist for the same mineral. Many of the reported data are not available as a standard reference for analytical purposes.

Having realized this, the experts of the field have recently called the attention to the necessity of making use of temperature dependence for the analysis of iron-bearing oxide minerals [32] as well as to use the distribution-extracting methods in mineral analysis [27].

3.1 Microenvironments—site determination

Site determination is a unique application of Mössbauer spectroscopy frequently used not only in mineralogy and geochemistry but in inorganic and organic chemistry, biochemistry, and metallurgy as well.

3.1.1 Qualitative analysis

Site determination by Mössbauer spectroscopy means the identification of the possible structural positions (microenvironments) as reflected by the elementary or superimposed patterns in a complex Mössbauer spectrum and the quantitative estimation of the fractions of Mössbauer atoms situated at structurally distinct positions in the same phase from the corresponding pattern areas (intensities). For this reason, the standard and induced patterns of a given mineral should be appropriately decomposed into elementary patterns, then the site assignment of the elementary patterns has to be given. The elementary patterns belonging to microenvironments in minerals are frequently doublets. These doublets have an isomer shift and quadrupole splitting systematics depending on the coordination number of iron.

Figure 14 shows the correlation between the coordination number and the isomer shift/quadrupole splitting of iron in different compounds. Site distortion from either octahedral or tetrahedral sym-

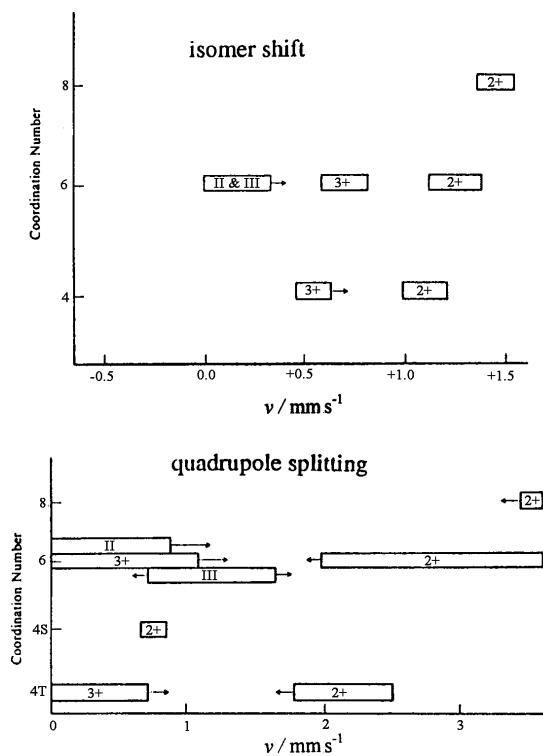


Fig. 14 Correlation between coordination number and isomer shift/quadrupole splitting for ^{57}Fe [13] as a function of its valence state. (2+ and 3+ indicate ionic, II and III covalent iron.)

metry can also be determined [13,33,34]. Iron in tetrahedral coordination can be distinguished from that in octahedral coordination on the basis of its lower isomer shift, which reflects higher covalency. Isomer shifts lower than 0.3 mm/s (not shown) can be diagnostic for high-spin Fe^{3+} in tetrahedral coordination. Nevertheless, the isomer shift of low-spin Fe^{3+} or Fe^{2+} can also be lower than 0.3 mm/s.

It is generally believed that the hyperfine interactions that are responsible for the individual elementary patterns (the latter representing different microenvironments of iron) are principally determined by the first nearest neighbors of the corresponding iron atoms*. Note that for a given crystallographic site, such a neighborhood consists mainly of anions, the arrangement of which (including symmetry and interatomic distances) only shows minor variations within the same group of minerals. Thus, the Mössbauer parameters of an elementary pattern may be indicative of a certain crystallographic site. For instance, the ^{57}Fe Mössbauer spectra of minerals can be decomposed to subspectra representing distinct crystallographic sites occupied by Fe^{2+} or Fe^{3+} , as in the case of the cited example of garnets in subsection 3.2.

3.1.2 Standard and induced patterns as elementary patterns

In the simplest case, standard and induced patterns are elementary patterns.

Figure 15 shows the induced pattern (recorded at 77 K) of a pyrope sample of the composition $(\text{Mg}_{2.8}\text{Ca}_{0.42}\text{Mn}_{0.03}\text{Fe}_{0.47}^{2+})(\text{Al}_{1.75}\text{Cr}_{0.25})[\text{SiO}_4]_3$ [35,36]. The spectrum consists of a single elementary pattern ($\delta = 1.34$ mm/s and $\Delta = 3.55$ mm/s) representing bivalent iron substitution at the dodecahedral position. On the other hand, the induced pattern of andradite, $\text{Ca}_3(\text{Al}_{0.04}\text{Fe}_{1.96}^{3+})[\text{SiO}_4]_3$, also consists of one elementary pattern only (a quadrupole doublet with $\delta = 0.42$ mm/s and $\Delta = 0.62$ mm/s), which is characteristic of trivalent iron at the octahedral position (see Fig. 16). These site assignments have been based on the isomer shift and quadrupole splitting systematics (Fig. 14) and supported by the results of other (analytical) measurements as well as by mineralogical expectations.

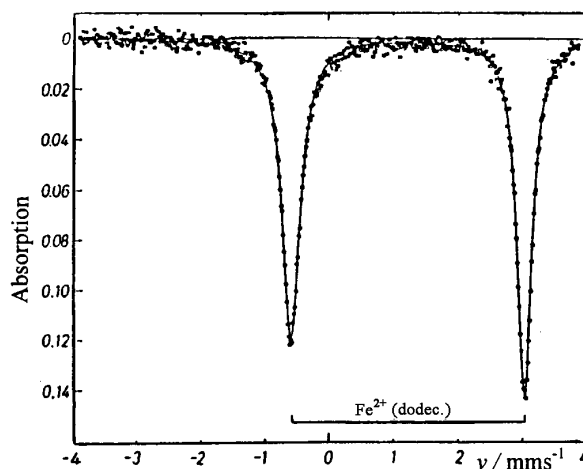


Fig. 15 Induced pattern of a pyrope $(\text{Mg}_{2.08}\text{Ca}_{0.42}\text{Mn}_{0.03}\text{Fe}_{0.47})(\text{Al}_{1.75}\text{Cr}_{0.25})[\text{SiO}_4]_3$ (recorded at 77 K) [35]. The doublet is associated with ferrous iron in dodecahedral position.

*In the case of several minerals, the effect of cations sitting in the second coordination shell should also be considered (see later).

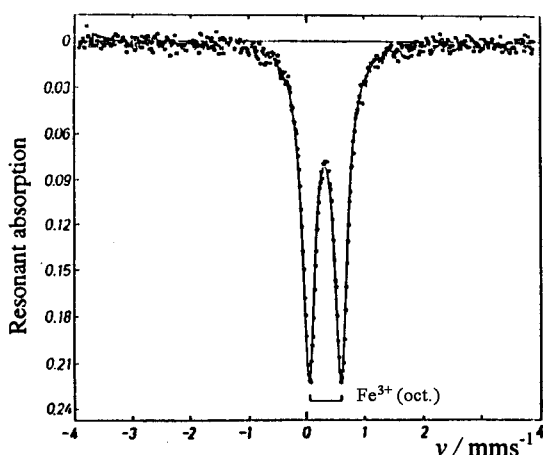


Fig. 16 Induced pattern (recorded at 77 K) of natural andradite $\text{Ca}_3(\text{Al}_{0.04}\text{Fe}_{1.96}^{3+})[\text{SiO}_4]_3$ [35]. The doublet is associated with ferric iron in octahedral position.

3.1.3 Standard and induced patterns as superimposed patterns

In the case of a superimposed pattern of the synthetic Ti andradite, $\text{Ca}_3(\text{Fe}^{3+}, \text{Ti}^{4+})[(\text{Si}, \text{Ti}^{4+}, \text{Fe}^{3+})\text{O}_4]_3$ (the induced and standard patterns of which are shown in Fig. 17), the octahedral (oct.) and tetrahedral (tet.) Fe^{3+} can also be distinguished very easily. In other cases, however, overlapping of the respective patterns makes their separation quite difficult, so a very careful analysis is required.

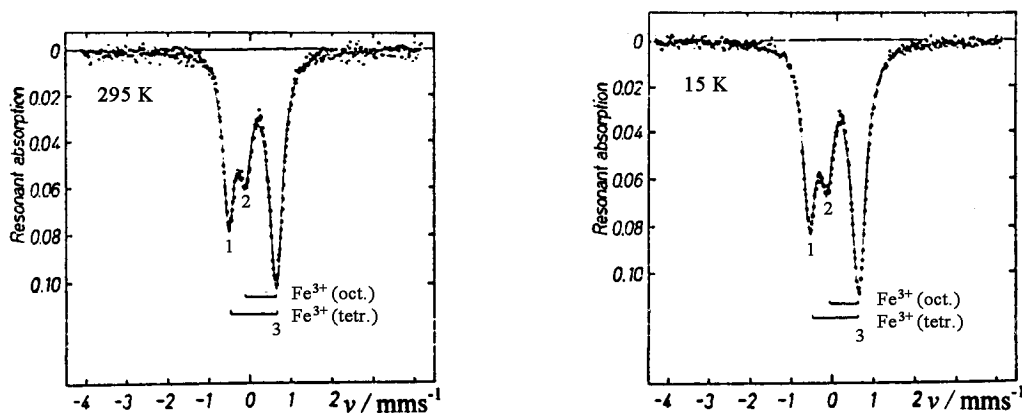


Fig. 17 Standard (left) and induced (right) pattern recorded at 295 K and 15 K, respectively, of Ti andradite [35]. The bars denote the peak separation in doublets belonging to Fe^{3+} in tetrahedral (tet.) and octahedral (oct.) positions.

3.1.4 Patterns with overlapping peaks

It is a common problem with Mössbauer spectra consisting of several quadrupole doublets that the patterns are hard to separate owing to the overlapping of the spectrum peaks.

The following example illustrates how to use induced patterns for solving this problem in the case of orthopyroxenes.

The standard pattern of an orthopyroxene can be seen in Fig. 18a. Considering the contour of this spectrum, it is evident that it reflects at least two doublets. However, owing to the high correlation between the individual peak parameters (which is the consequence of the overlapping peaks), the four

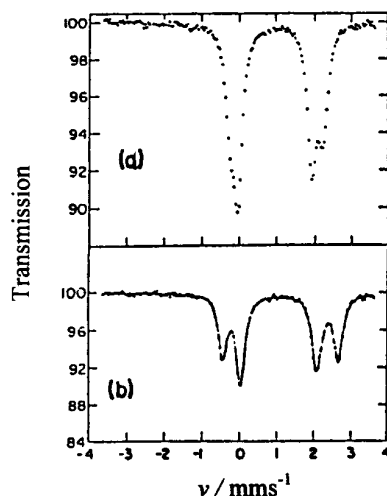


Fig. 18 Standard pattern (a) and induced pattern (b) of an orthopyroxene sample [35]. The induced pattern was recorded at 77 K, where the doublets are well resolved. The inner doublet belongs to ferrous iron in M2 position, while the outer doublet reflects ferrous iron in M1 position.

peaks cannot be assigned to the two doublets with 100 % certainty. (Of course, there are always some combinations, which can be excluded on grounds of the resulting unusual isomer shifts.)

By recording the induced patterns at different temperatures (see at 77 K in Fig. 18b), the temperature dependence of quadrupole splitting and isomer shift of the well-resolved doublets makes it quite clear which peak belongs to which doublet.

However, the assignment of the doublets to the M1 and M2 positions of the pyroxene structure has not yet been solved at this stage. In order to find out which doublet belongs to which site, we can use the site population data determined by other methods, e.g., by X-ray diffractometry. The concentration dependence of the quadrupole splitting of the M1 and M2 sites can be used for concentration calibration (Fig. 19). Site assignment can also be supported by the theoretical calculation of quadrupole splitting involving the estimation of the electric field gradient [13,33,34,36].

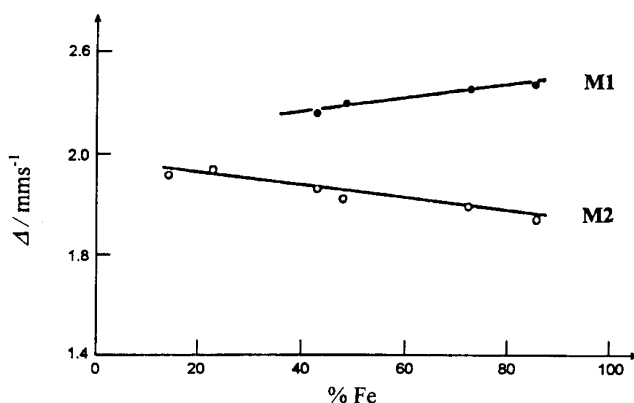


Fig. 19 Correlation between the quadrupole splitting and composition of orthopyroxenes at the M1 and M2 positions [37].

Another example for overlapping peaks is shown in Fig. 20 representing the standard (room-temperature) spectrum of augite, $(\text{Ca,Fe,Mg})_2\text{Si}_2\text{O}_6$, decomposed to three elementary patterns (i.e., three doublets). The doublets are represented by pairs of peaks with asymmetric areas as an indication of the sample being textured. The individual subspectra reflect different crystallographic sites occupied by Fe^{2+} and Fe^{3+} . It is easy to recognize from the corresponding isomer shift values that doublets D_1 and D_2 must be attributed to Fe^{2+} , while doublet D_3 is associated with Fe^{3+} . The assignment of elementary patterns is done by considering the crystal structure of the given mineral, the results of other measurements and by comparing its Mössbauer spectrum with those of other pyroxenes having different cation concentrations. In pyroxenes, both of the distinct cation sites M1 and M2 can be occupied by Fe^{2+} and Fe^{3+} . In the spectrum of augite (Fig. 20), doublet D_1 ($\delta = 1.4$ mm/s, $\Delta = 2.44$ mm/s) is due to Fe^{2+} in M1, doublet D_2 ($\delta = 1.4$ mm/s, $\Delta = 1.96$ mm/s) is due to Fe^{2+} in M2, and doublet D_3 ($\delta = 0.7$ mm/s, $\Delta = 0.59$ mm/s) is due to Fe^{3+} in M1 and/or M2 positions. Since the isomer shift and quadrupole splitting of Fe^{3+} are less sensitive to a change in the coordination geometry than those of Fe^{2+} , it is not possible to distinguish between the Mössbauer patterns of Fe^{3+} in the M1 and M2 positions [13,34].

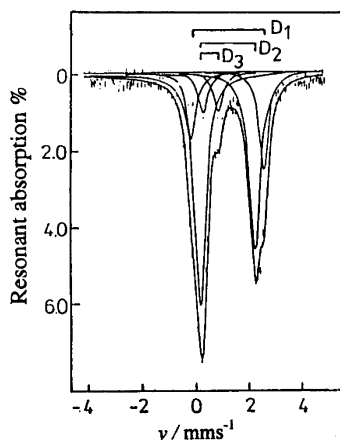


Fig. 20 Standard pattern of augite [38] recorded at room temperature. The site assignment of the doublets is: D_1 is due to Fe^{2+} in M1, D_2 is due to Fe^{2+} in M2, and D_3 is due to Fe^{3+} in M1 or M2.

A further example for overlapping peaks is amphibole. In the amphibole structure, there are four octahedral sites for Fe^{2+} (M1, M2, M3, and M4), out of which three are situated within the ribbon (M1, M2, and M3) and the fourth, more distorted one (M4), along the edges. The subspectrum representing Fe^{2+} in the Mössbauer spectrum of amphiboles (Fig. 21) can only be decomposed to two doublets. One of them is associated with iron at either of the three similar positions (M1, M2, and M3), while the other represents iron occupying the M4 site. If the spectra are recorded with extremely high statistics, however, it is sometimes possible to distinguish [39] between the M1, M2, and M3 positions as illustrated by Fig. 22.

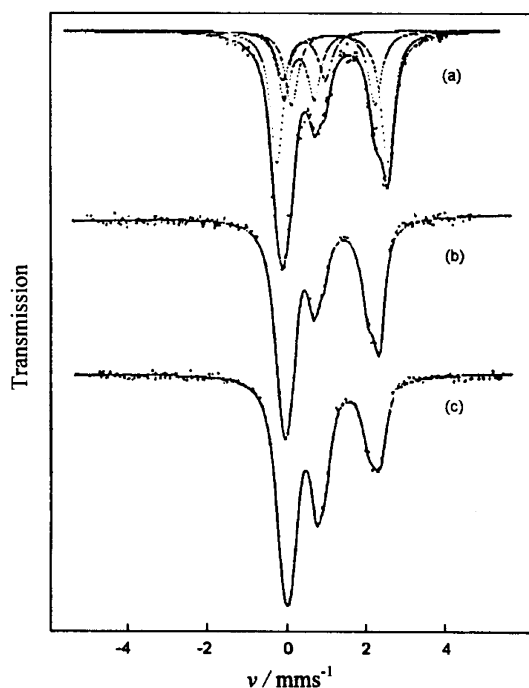


Fig. 21 Standard patterns of amphibole megacrysts from different locations in the Carpathian Basin [39]. (a) Burgenland, (b) Nógrádgyömör, (c) Balaton Highland.

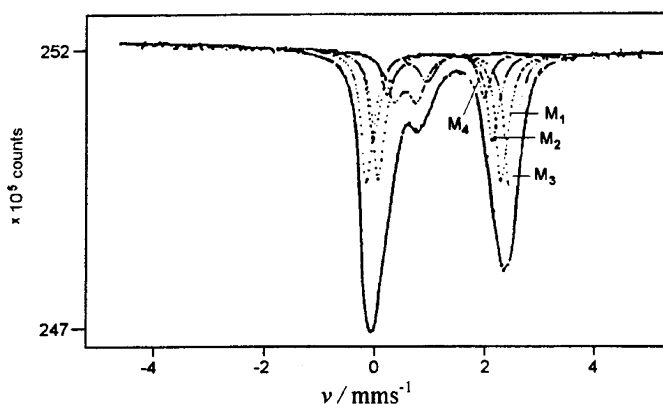


Fig. 22 Room-temperature Mössbauer spectrum of an amphibole sample from Mecsek Mts., Hungary. The Mössbauer spectrum was recorded with unusually high statistics [39]. This made it possible to resolve the spectrum into Fe^{2+} doublets corresponding to M1, M2, M3, and M4 positions, separately. The low-intensity doublets belong to two Fe^{3+} sites.

3.1.5 Quantitative site analysis

The quantitative site occupancy analysis is based on the determination of the pattern area (intensity) belonging to the individual sites in the mineral. In the most general case, we have n nonequivalent crystallographic positions that are partially occupied by the studied Mössbauer element, say iron. Let x_i denote the fraction of iron atoms (either Fe^{2+} or Fe^{3+}) that occupy the i^{th} site (site occupancy). Now x_i can be obtained from the pattern areas as follows:

$$x_i = \frac{d_i A_i}{\sum_{j=1}^n d_j A_j} \quad (36)$$

where A_i is the pattern area (intensity) of iron occupying the i^{th} crystallographic position and d_i is a coefficient including among others the reciprocal of the respective Mössbauer–Lamb factor. (Thus, the reciprocal of d_i expresses the sensitivity of the Mössbauer method for iron atoms sitting at the i^{th} crystallographic site.)

For example, the site occupancy of Fe^{3+} has been determined [35] by the above-indicated way for the octahedral and the tetrahedral sites in the synthetic Ti andradite, $\text{Ca}_3(\text{Fe}^{3+}, \text{Ti}^{4+})[(\text{Si}, \text{Ti}^{4+}, \text{Fe}^{3+})\text{O}_4]_3$, the standard and induced patterns of which are shown in Fig. 17.

3.1.6 Neighbor effects

In most minerals, the cations are situated in a close-packed oxygen or sulfur structure, and therefore their first coordination shells show little variation in composition. The structure of native alloys (e.g., some meteorites) is different. For this reason, the effect of the variation of the first neighbors should be considered here. However, the variation of the composition of the second shell plays an important role in the case of several complex oxides and silicates.

The following method can be used for the interpretation of the Mössbauer spectra of alloys [40] and mixed oxides.

The occurrence of iron in the different cation neighborhoods can be calculated from the statistical distribution of the coordination spheres having different compositions. In the case of a solid solution, one usually assumes random substitution resulting in the polynomial (or, in the simplest binary case, the binomial) distribution of the different neighborhoods. For example, in a random binary alloy, the fraction of sites occupied by iron atoms, the neighborhood of which happens to consist of k iron atoms and $(N-k)$ alloying atoms, is given by the binomial distribution

$$P(k; N) = \binom{N}{k} x^k (1-x)^{N-k}, \quad (37)$$

where N is the total number of atoms in the nearest neighborhood of the selected site and x is the atomic fraction of iron.

This gives a possibility to check by Mössbauer spectroscopy whether the chances of having k iron neighbors out of the N reflect statistically random substitution or not, because the relative areas of the individual subspectra are practically equal to the corresponding fractions of iron having different surroundings.

Omphacite, $(\text{Ca}, \text{Na})(\text{Mg}, \text{Fe}, \text{Al})\text{Si}_2\text{O}_6$, gives an example for the effect of the variation of the composition of the second coordination shell. Its spectrum (Fig. 23) can be decomposed to four doublets. The doublet with the smallest isomer shift and quadrupole splitting can be associated unambiguously with Fe^{3+} , and the remaining three reflect Fe^{2+} microenvironments. In the earliest study [41], the ferrous subspectra were attributed to different crystallographic sites, which site assignment is in contradiction with the X-ray results. Namely, the iron atoms occupy the M1 site in the structure [21]. Thus, the three ferrous doublets were correctly associated with iron atoms at the M1 site having different configurations of Ca^{2+} and Na^+ ions in the more spacious three neighboring M2 sites [42]. Accordingly, the doublets with $\Delta = 1.85$ mm/s, 2.22 mm/s, and 2.76 mm/s were associated with iron atoms at the M1 site having neighbors of 3 Ca^{2+} and 0 Na^+ , 2 Ca^{2+} and 1 Na^+ , and 1 Ca^{2+} and 2 Na^+ , respectively.

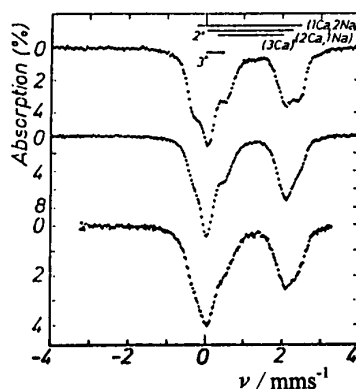


Fig. 23 Natural pattern of different omphacite samples [21]. The subspectra represent Fe^{2+} at M2 site having different distribution of neighboring cations.

Table 1 shows the fractions of ferrous ions found in different environments characterized by particular combinations of Ca^{2+} and Na^+ neighbors at the M2 sites of omphacite. The comparison of these fractions derived from the measured spectra with those calculated on the basis of binary distribution clearly demonstrates a preference of the ferrous environments with an odd number of Ca^{2+} neighbors.

Table 1 Relative probabilities of a ferrous ion being found in omphacites in an environment with a particular combination of Ca and Na neighbors on M2 sites, derived from the spectra of Fig. 23 (obs.) or calculated on the basis of a random distribution of Ca and Na (calc.).

| Neighbor configuration | Sample 1 | | Sample 2 | | Sample 3 | |
|------------------------|----------|-------|----------|-------|----------|-------|
| | obs. | calc. | obs. | calc. | obs. | calc. |
| 3Ca | 0.33 | 0.21 | 0.32 | 0.32 | 0.30 | 0.33 |
| 2Ca1Na | 0.23 | 0.43 | 0.37 | 0.44 | 0.43 | 0.44 |
| 1Ca2Na | 0.44 | 0.29 | 0.31 | 0.21 | 0.27 | 0.20 |
| 3Na | – | 0.07 | – | 0.03 | – | 0.03 |

A number of doublets with different quadrupole splittings can be considered as representing a special (discrete) type of quadrupole splitting distribution. The quadrupole splitting distributions—special types of transformed patterns—can be derived from the measured spectra using special computer programs. The transformed patterns are especially important when there is a large number of configurations reflecting different neighborhoods [40], and when the difference between the quadrupole splittings characterizing the different configurations is smaller than the peak width. In such cases, an appropriate decomposition of transformed patterns can help find the most probable configurations at which the iron can exist in the system.

The evaluation of the quadrupole splitting distributions of certain minerals—for which the decomposition of the Mössbauer spectra to doublets representing distinct iron positions appears to be quite satisfactory—shows that the distribution peaks are wider than the expected* peak widths of the natural pattern. This “extra distribution” can be due to the existence of different microenvironments, i.e., different configurations in the second coordination shell of the iron. This effect may cause an apparent peak broadening in the Mössbauer spectra. Consequently, a careful analysis is needed—involving

*That is, the peak widths expected from the absorber thickness and from geometrical effects.

ing the comparison of the transformed and the induced patterns—to decide whether a peak broadening that appears in the standard pattern of a mineral requires further considerations.

The disturbing effect of texture on the relative peak areas (often occurring in minerals due to perfect or good cleavage) should also be taken into consideration while evaluating spectra. Texture causes an asymmetry in the area of the doublet peaks (see subsection 1.2) and also affects the relative peak areas within a sextet. Having an axial texture (which is the most common situation with powder samples), one can eliminate its effect by measuring the sample at the “magic” angle 55° between the normal vector of the plane of the sample and the direction of the γ -rays [43]. Alternatively, the powder can be mixed in a neutral and viscous matrix of low atomic number, such as paraffin or petroleum jelly, to get a uniform (i.e., random) distribution of crystallographic directions.

The reliability of quantitative analysis by Mössbauer spectroscopy depends very much on the precision of peak-area determination. The detection limit of area determination in a complex Mössbauer spectrum is a few percent. The accuracy of Mössbauer analysis can be enhanced by recording the spectrum up to higher counts resulting in a lower relative standard deviation.

Nevertheless, despite the possible ambiguities, valuable information concerning site population of iron in minerals can often be obtained by Mössbauer spectroscopy, when it is not obtainable by other methods.

3.2 Microenvironment—valence state determination

One of the most successful fields of Mössbauer spectroscopy in earth sciences is the absolute/relative valence state determination of cations in minerals. For example, in several iron-containing minerals, the most accurate determination of the $\text{Fe}^{3+}/\text{Fe}^{2+}$ ratio can be performed by Mössbauer spectroscopy. This is so because the standard techniques either cannot distinguish between Fe^{2+} and Fe^{3+} at all (routine X-ray fluorescent and routine electron microprobe analysis), or they can only provide inaccurate $\text{Fe}^{3+}/\text{Fe}^{2+}$ ratio (wet chemical analysis). The valence state of iron is of considerable mineralogical and geological importance as it is related to the formation of minerals under different conditions as well as to their oxidation, weathering, color, and pleochroism, etc.

3.2.1 Isomer shift systematics of microenvironments

The valence state of a Mössbauer nuclide is basically determined from its isomer shift δ , characteristic of the given microenvironment.

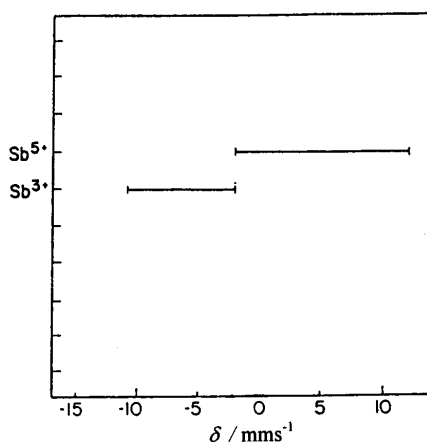


Fig. 24 Correlation between the oxidation state and isomer shift for ^{121}Sb [8]. The valence state Sb^{3+} can be well distinguished from the oxidation state Sb^{5+} using the isomer shift.

It follows from eq. 1 that the isomer shifts of different absorber materials will be different, since the electronic density changes from one microenvironment to the other. Thus, the isomer shift is affected by oxidation state and by the occupation number of electronic orbitals.

Figures 24–27 show the correlation between isomer shift and oxidation state for some of the Mössbauer nuclides (^{57}Fe , ^{119}Sn , ^{121}Sb , ^{151}Eu) that are most frequently used as probes in Mössbauer spectroscopic studies. As we can see, the determination of isomer shift makes it possible to distinguish between Sn^{2+} and Sn^{4+} , Sb^{3+} and Sb^{6+} , Eu^{2+} and Eu^{3+} , as well as between Fe^{2+} and Fe^{3+} . Moreover,

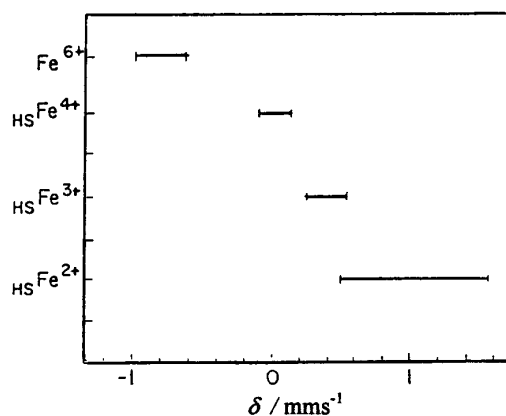


Fig. 25 Correlation between the oxidation state and isomer shift for ^{57}Fe [8]. The oxidation states of high-spin (HS) iron states can be well distinguished using the isomer shift.

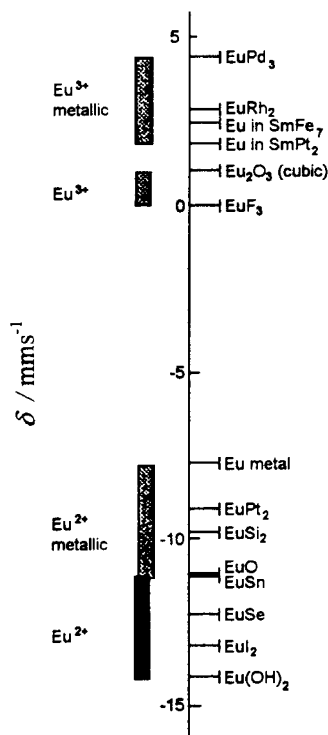


Fig. 26 Correlation between the oxidation state and isomer shift for ^{151}Eu [8]. The Eu^{3+} can be excellently distinguished from Eu^{2+} using the isomer shift, because the gap between typical values is as high as 10 mm/s.

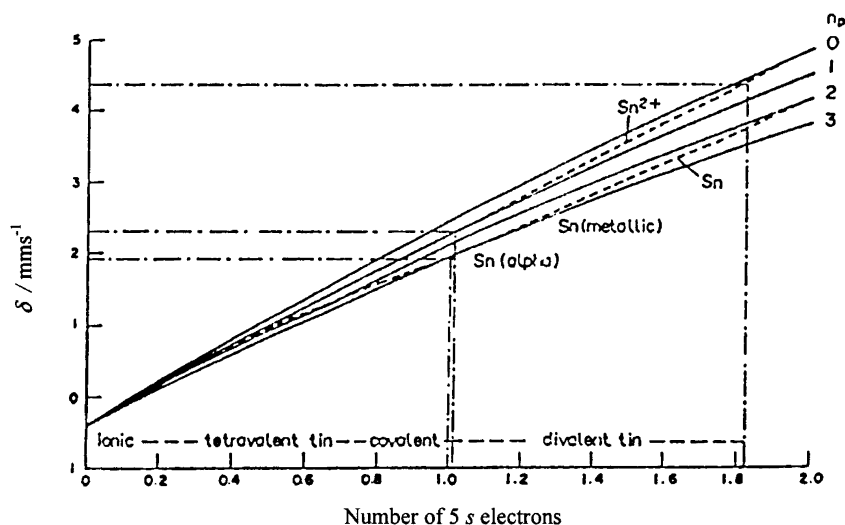


Fig. 27 Correlation between the oxidation state and isomer shift for ^{119}Sn [8]. Not only the oxidation states of Sn^{2+} and Sn^{4+} can be well distinguished, but the effective number of 5s and 5p (n_p) electrons can also be determined from the isomer shift.

it is also possible to distinguish high-spin iron from low-spin iron provided that the oxidation state is known.

In the case of ^{119}Sn , ^{121}Sb , and ^{151}Eu , the typical isomer shift ranges of the different valence states are neatly separated. This is a consequence of the fact that the electronic density at the nucleus of these nuclides is determined by the number of valence s electrons. One can also observe that the higher the valence state, the lower the isomer shift. This is so because the factor α in eq. 1 is positive for these nuclides, and therefore the removal of s electrons (this happens when we go to higher valence state from the lower one) will decrease the electronic density at the nucleus and thus the isomer shift as well.

In the case of ^{57}Fe , the electronic density at the nucleus (and so the isomer shift) depends both on the number of 4s electrons (which are actually present in the nucleus) and on the number of 3d electrons (which decrease the s electron density in the nucleus by shielding the nuclear charge). Consequently, the isomer shift ranges typical of different valence and spin states will overlap each other considerably (Fig. 28). Thus, low-spin Fe^{3+} and Fe^{2+} cannot be distinguished from each other by the isomer shift alone*, however, in most cases the problem can be solved by considering the characteristic values of the quadrupole splitting [3,11,13,44].

The electronic densities can be theoretically calculated for different electronic configurations [8]. A correspondence between the isomer shift and electronic configuration of iron is illustrated in Fig. 29 [45].

The determination of isomer shift is also very important for the separation of the various micro-environments (see Section 3.1).

*Fortunately, minerals are typically high-spin substances.

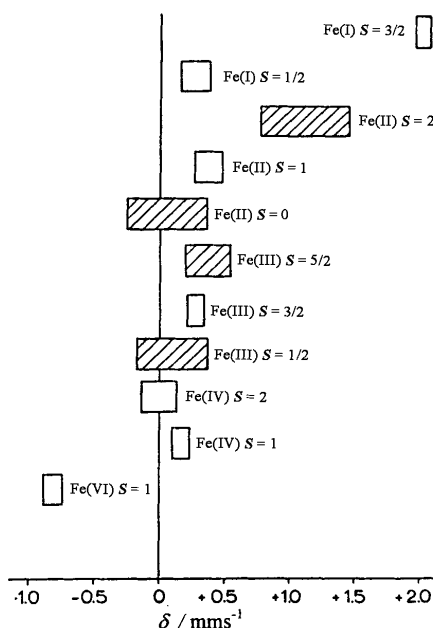


Fig. 28 Isomer shift ranges typical of different valence and spin states for ^{57}Fe [13]. The most common configurations are indicated by shadowed regions. The low-spin Fe^{3+} and Fe^{2+} , which states are rarely found in minerals, cannot be distinguished using the isomer shift data alone, however, the characteristic difference between the quadrupole splitting values can solve the ambiguity. S denotes the resulting spin of 3d electrons.

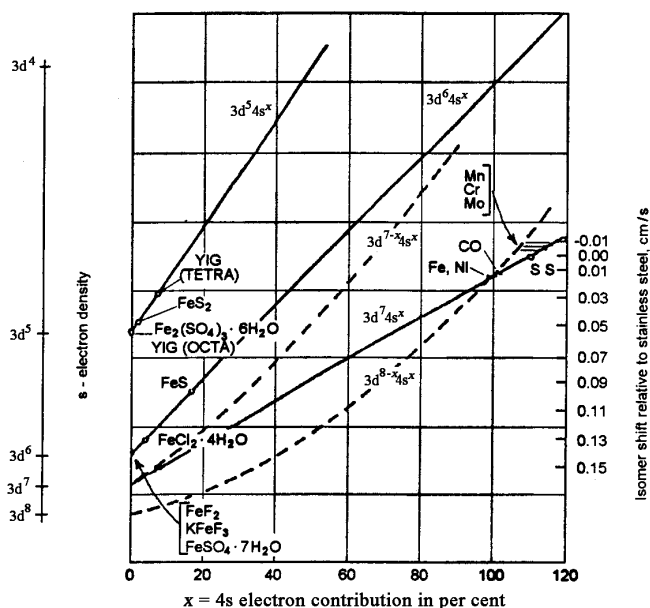


Fig. 29 Interpretation of ^{57}Fe isomer shifts [45]. The observed isomer shifts (on the right ordinate) for most ionic Fe^{3+} and Fe^{2+} compounds are associated with the total s electronic density (on the left ordinate) and with 4s electronic population (on the abscissa). The electronic densities were theoretically calculated taking into consideration the shielding effect of 3d electrons on 3s electrons for different $3d_n 4s_x$ configurations. This diagram can be used to estimate the electronic density from the isomer shift at a given configuration.

3.2.2 Determination of the $\text{Fe}^{2+}/\text{Fe}^{3+}$ ratio

The Fe^{2+} and Fe^{3+} states very often occur together in garnets, as illustrated in Fig. 30 showing the 77 K ^{57}Fe Mössbauer spectrum of a pyrope sample $(\text{Mg},\text{Fe}^{2+})_3(\text{Al},\text{Fe}^{3+})_2[\text{SiO}_4]_3$. (The ferrous iron is at the dodecahedral position, and the ferric ion is at the octahedral.) In this case, the $\text{Fe}^{2+}/\text{Fe}^{3+}$ ratio could be determined by using the relative areas of the elementary patterns representing the microenvironments of Fe^{2+} and Fe^{3+} . The quantitative analysis is based on the thin-absorber approximation expressed by eq. 35. As to the quantitative determination of the $\text{Fe}^{2+}/\text{Fe}^{3+}$ ratio, it should be considered that, at low measuring temperatures (i.e., below 77 K), the area ratios of different Mössbauer species (e.g., those representing Fe^{2+} and Fe^{3+} ions, like in the present case) give a very good approximation for the atomic ratios represented by them. However, the vibrational amplitudes (and thus the Mössbauer–Lamb factors that play an important part in converting atomic/ionic fractions to relative areas) may have different temperature dependences as a result of which the area fractions obtained at higher temperature (e.g., at room temperature) will give a poorer approximation for the ionic fractions unless appropriate corrections are made [13,35]. This possibility is well supported by the last column of Table 2 showing the unequal change of the f factors.

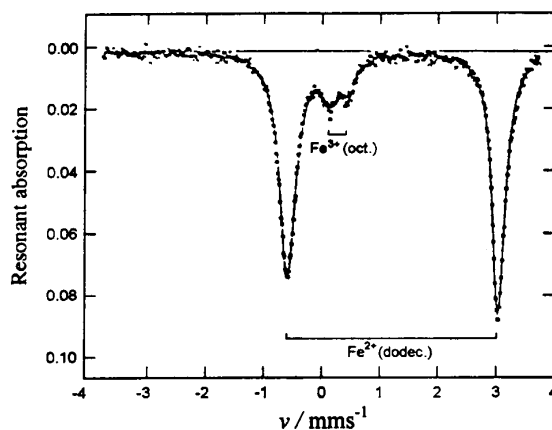


Fig. 30 Induced pattern of a typical natural pyrope sample [35]. The Mössbauer spectrum was recorded at 77 K. The inner doublet belongs to ferric iron in octahedral (oct.) position while the outer one represents ferrous iron in dodecahedral (dodec.) position.

Table 2 Area ratios of iron species with different coordination in garnets [35].

| Garnet | Temperature T/K | Area fractions | | $r_{c,a}^{(T_2,T_1)}$ |
|-----------|-----------------------------|----------------------------------|--------------------------------|-----------------------|
| | | Fe^{2+} 24c (dodec.) | Fe^{3+} 16a (oct.) | |
| Pyrope | 4.5 | 0.871 | 0.129 | |
| | 77 | 0.862 | 0.138 | 0.93 ± 0.05 |
| | 295 | 0.840 | 0.161 | 0.77 ± 0.05 |
| Grossular | 4.5 | 0.212 | 0.788 | |
| | 77 | 0.196 | 0.805 | 0.91 ± 0.05 |
| | 295 | 0.168 | 0.832 | 0.75 ± 0.05 |

$$r_{i,j}^{(T_2,T_1)} = \frac{A_i^{(T_2)}/A_i^{(T_1)}}{A_j^{(T_2)}/A_j^{(T_1)}} = \frac{f_i^{(T_2)}/f_i^{(T_1)}}{f_j^{(T_2)}/f_j^{(T_1)}}$$

Mössbauer spectroscopy is an excellent tool for the determination of the $\text{Fe}^{2+}/\text{Fe}^{3+}$ ratio in minerals. The $\text{Fe}^{2+}/\text{Fe}^{3+}$ ratio determined by Mössbauer spectroscopy is more reliable than that obtained by wet chemical analysis, because the preparation of Mössbauer samples does not affect their chemical state. Wet chemical analysis can give lower $\text{Fe}^{2+}/\text{Fe}^{3+}$ value than the correct one owing to oxidation that may occur during the suspension or grinding of the minerals in the preanalytical manipulation. However, it can also yield higher ratio owing to the errors in the standard determination when the total iron content and the Fe^{2+} content are measured by different procedures.

Several studies have dealt with the comparison of the $\text{Fe}^{2+}/\text{Fe}^{3+}$ ratios obtained by Mössbauer spectroscopy and by wet chemical analysis [33,46]. Generally, the results correlate well for sheet silicates [46], but the mentioned factors influence the correlation. The deviation is particularly significant, if one of the valence states is dominant and/or if the total amount of iron is too low in the sample. In such cases, even a small absolute error of any of the steps of wet chemical analysis can result in unrealistic $\text{Fe}^{2+}/\text{Fe}^{3+}$ ratios.

As we have seen, the valence state can be determined fairly satisfactorily by conventional Mössbauer spectroscopy. However, the assignment of elementary patterns to microenvironments is not always easy, since the isomer-shift ranges of the different valence states overlap each other. In the case of a complex superimposed spectrum consisting of many patterns, one must therefore consider it very carefully whether the elementary patterns extracted by the computer program are real fingerprints of the different valence states or just mathematical artifacts.

3.3 Microenvironment—characterization of magnetic state

Mössbauer spectroscopy is an excellent tool for the characterization of magnetism in iron-bearing minerals. In this case, the microenvironments are also determined by the magnetic interactions. This is so because with magnetically ordered (nonsuperparamagnetic) minerals the Mössbauer pattern shows a magnetic splitting below the temperature of magnetic ordering. The magnetic splitting, on the other hand, reflects the magnitude and the direction of the effective magnetic flux density at the nucleus of iron. Owing to this, we can determine the direction of magnetic moments in oriented single crystals.

Mössbauer spectroscopy can be used to study the general nature of magnetic ordering and magnetic coupling in minerals. In other words, it can help determine whether a mineral is ferromagnetic, ferrimagnetic, or antiferromagnetic, since the induced patterns are characteristic and indicative of the different magnetic couplings. Such established patterns can then be used as fingerprints for the analysis of magnetic materials.

In order to determine the type of magnetic ordering, a polycrystalline sample has to be measured in an external magnetic field. If the direction of the external field is parallel to that of the Mössbauer γ -rays, the $\Delta m = 0$ transitions (represented by the second and fifth peaks of a sextet) will vanish for ferromagnetic and ferrimagnetic materials (see Fig. 2 and eq. 17).

- In the case of **ferromagnetic** materials, external magnetic fields do not introduce additional magnetic splitting in the Mössbauer spectra.

- With **ferrimagnetic** materials, two magnetically split subspectra exist even without an external field. When an external field is applied, it will increase or decrease the magnitude of the effective magnetic flux density depending on whether the direction of the external field is parallel or antiparallel to that of the internal field at the given sublattice.


- With polycrystalline **antiferromagnetic** materials, the external field (set parallel to the direction of Mössbauer radiation) will not change the ratio of peak areas. Thus, antiferromagnets can be easily distinguished from ferromagnets and ferrimagnets.

- The determination of more **complex magnetic structures** (e.g., canted, helical, spiral, and modulated antiferromagnetic structures) can also be elucidated by Mössbauer spectroscopy using oriented

samples (i.e., single crystals or textured polycrystals), external magnetic fields, and polarization γ -spectroscopy [5,18].

Table 3 shows the orientation of spins and their interactions reflected by Mössbauer spectroscopy in the case of common magnetic structures.

Table 3 Orientation of spins in different magnetic structures.

| Ferromagnetic | Antiferromagnetic | Ferrimagnetic | Canted antiferromagnetic (weak ferromagnetic) |
|---|--|---|---|
| $\uparrow\uparrow$ $\uparrow\uparrow$ | $\uparrow\uparrow$ $\downarrow\downarrow$ | $\uparrow\uparrow$ $\downarrow\downarrow$ |  |
| No splitting of the spectral peaks in an applied field. | Splitting of the spectral peaks in an applied field directed along the antiferromagnetic axis. Sharp spin reorientation. | Distinct magnetically split spectra with different hyperfine fields*. | Splitting of the spectral peaks in an applied field directed along the antiferromagnetic axis. Continuous spin reorientation. |

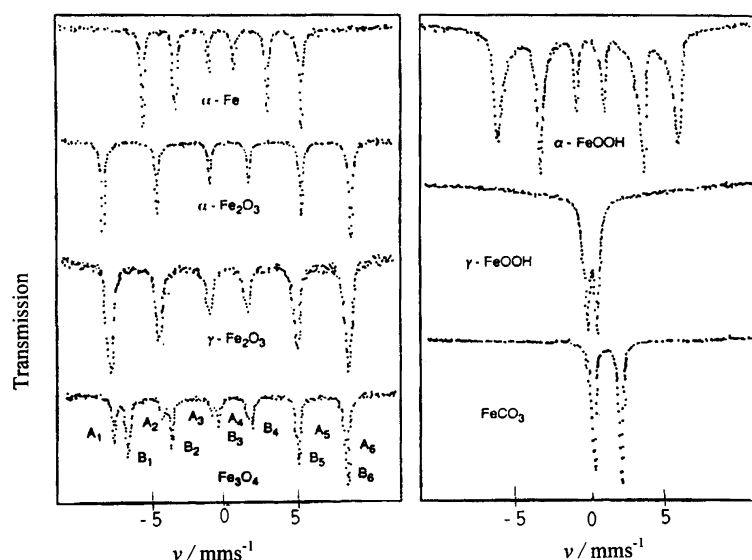


Fig. 31 Standard patterns of different iron compounds as well as native iron [20].

The magnetic ordering temperature of minerals can be determined from the temperature dependence of the Mössbauer spectra. Since the magnetic splitting collapses at the transition temperature, the latter can be determined from the effective magnetic flux density vs. temperature diagram by extrapolating to $B = 0$.

3.3.1 Ferromagnetism

Ferromagnetic ordering can be observed in the Fe and Fe–Ni alloys of iron meteorites. Figure 31 shows the Mössbauer spectrum of α -iron. The symmetric six-peak pattern—the quadrupole splitting is zero due to the bcc structure—reveals an effective magnetic flux density of 33.0 T at room temperature. In the case of Fe–Ni alloys, the introduction of the alloying element Ni into the iron matrix will cause a

*That is, with different values of magnetic flux density at the nucleus.

perturbation in the charge and spin density. This can be detected by Mössbauer spectroscopy, because the perturbation causes changes in the effective magnetic field and the isomer shift.

3.3.2 Ferrimagnetism

The most frequently studied ferrimagnetic mineral is magnetite. In the case of magnetite, ferrimagnetism is the result of two magnetic orderings. Namely, there is an antiferromagnetic ordering of Fe^{3+} occupying the octahedral sites and there is a ferromagnetic ordering of Fe^{2+} at the tetrahedral sites. This is well reflected by the room-temperature Mössbauer spectrum of magnetite (Fig. 31) consisting of two sextets with different effective magnetic flux densities and isomer shifts (see Table 4).

Table 4 Mössbauer parameters of iron oxides and hydroxides.

| Compound | Position | Measurement T/K | $\delta/\text{mm s}^{-1}$ | $\Delta/\text{mm s}^{-1}$ | B/T | Magnetic trans. T/K |
|--|----------------------------|--------------------|---------------------------|---------------------------|------|------------------------|
| $\alpha\text{-FeOOH}$ | – | 0 | – | – | 51.0 | 393.3 |
| | – | 80 | – | – | 50.0 | – |
| | – | 300 | +0.40 | – | 36.7 | – |
| $\beta\text{-FeOOH}$ | – | 80 | +0.47 | 0.11 | 47.6 | 295 |
| | – | 300 | +0.38 | 0.53 | – | – |
| | – | – | +0.39 | 0.88 | – | – |
| $\delta\text{-FeOOH}$ | – | 80 | – | – | 52.5 | – |
| | – | 300 | +0.35 | 0.60 | – | – |
| $\gamma\text{-FeOOH}$ | – | 77 | +0.52 | – | – | – |
| | – | 295 | +0.38 | 0.60 | – | – |
| $\text{Fe}(\text{OH})_2$ | – | 95 | +1.36 | 3.13 | – | – |
| $\text{Fe}(\text{OH})_3$ | – | 300 | +0.37 | 0.51 | – | – |
| | – | – | +0.37 | +0.85 | – | – |
| $\text{Fe}(\text{OH})_3 \cdot n\text{H}_2\text{O}$ | – | 300 | +0.37 | 0.64 | – | – |
| FeO | – | 295 | +0.93 | 0.8 | – | 198 |
| Fe_3O_4 | Fe^{3+} (tet.) | 298 | +0.27 | 0.01 | 49.3 | – |
| | | 77 | +0.44 | 0 | 51.4 | – |
| | | 4.2 | +0.042 | –0.06 | 51.6 | – |
| | $\text{Fe}^{2+/3+}$ (oct.) | 298 | +0.67 | 0.04 | 46.0 | – |
| | | 77 | +0.94 | +0.76 | 49.9 | – |
| | | 4.2 | +0.99 | –0.89 | 51.0 | – |
| $\text{Fe}_{2-x}\text{O}_4$ | Fe^{3+} (tet.) | 300 | +0.39 | 0.11 | 50.3 | – |
| | $\text{Fe}^{2+/3+}$ (oct.) | 300 | +0.78 | 0.28 | 46.5 | – |
| $\alpha\text{-Fe}_2\text{O}_3$ | – | 296 | +0.39 | +0.24 | 51.5 | 956 |
| | – | 83 | – | –0.06 | 54.2 | – |
| $\gamma\text{-Fe}_2\text{O}_3$ | – | 300 | +0.43 | 0.06 | 50.6 | – |

3.3.3 Antiferromagnetism

Hematite is antiferromagnetically ordered at room temperature. The Mössbauer spectrum (Fig. 31) exhibits a well-resolved sextet with a characteristic effective magnetic flux density of 51.5 T and a considerable quadrupole splitting (see Table 4).

Antiferromagnetic interaction has been studied in different iron-containing spinels by Mössbauer spectroscopy. A considerable contribution to our knowledge of the magnetic structure of garnets has also been derived from Mössbauer measurements [47,48].

Mössbauer spectroscopy has revealed antiferromagnetic interaction in many silicates at low temperature [49–51]. The magnetic ordering temperatures of some silicates can be seen in Table 5.

Table 5 Magnetic ordering (Neel) temperatures for iron-rich silicate minerals.

| Mineral | T_N/K |
|----------------------------|---------|
| <i>1:1 layer silicates</i> | |
| Greenalite | 17 |
| Berthierine | 9 |
| Cronstedtite | 12 |
| <i>2:1 layer silicates</i> | |
| Ferripyrophyllite | 18 |
| Minnesotaitite | 20 |
| Glauconite | ~4 |
| Nontronite | 2 |
| Biotite | 7 |
| Thuringite | ~4 |
| <i>Pyroxenes</i> | |
| Orthoferrosilite | 37 |
| <i>Amphiboles</i> | |
| Grunerite | 23 |
| Riebeckite | 23 |
| Crocidolite | 30 |
| <i>Group silicates</i> | |
| Fayalite | 66 |
| Laihunite | ~80 |
| Staurolite | 6 |
| Ilvaite | 90 |

Figure 32 and Table 6 show the 4.2 K induced patterns and the related hyperfine parameters of greenalite, cronstedtite, minnesotaitite, ferripyrophyllite, crocidolite, and ilvaite. The spectra can be decomposed to magnetically split subspectra representing four- and six-coordinated Fe^{3+} and Fe^{2+} micro-environments. For both chain and sheet silicates, the dominant exchange interaction is ferromagnetic. However, in sheet silicates, a weak antiferromagnetic coupling also exists between the ferromagnetic sheets built from octahedral units. (The magnetic moments of the sheets lie in the plane.)

Mössbauer spectroscopy also indicates that antiferromagnetic coupling is stronger in chain silicates than in sheet silicates, because the ferromagnetic layers are closer to each other.

3.3.4 Magnetic relaxation

In this case, not a static, but a dynamically changing microenvironment should be considered.

Magnetic relaxation can be best understood considering paramagnetic materials. In a paramagnet, the fluctuation of the internal magnetic field at the nucleus is so fast (owing to fast spin–spin and spin–lattice relaxation) that only an average zero value can be observed over the time scale of the Mössbauer transition (10^{-8} s). However, when the relaxation of the paramagnetic spin is slow enough in comparison with the time scale of the Mössbauer transition and the frequency of the Larmor precession [17], a magnetic splitting appears in the Mössbauer spectrum even in the case of paramagnetic materials. The process of relaxation can be followed by Mössbauer spectroscopy [17,52].

Figure 33 shows the temperature dependence of the Mössbauer spectra of a limonite sample containing goethite and quartz as main components [50] of which only goethite is reflected in the spectrum. At room temperature (f), the sample shows the characteristic spectrum of poorly crystallized goethite. At low temperature, we have a sextet with broadened peaks which gradually collapses inwards as the

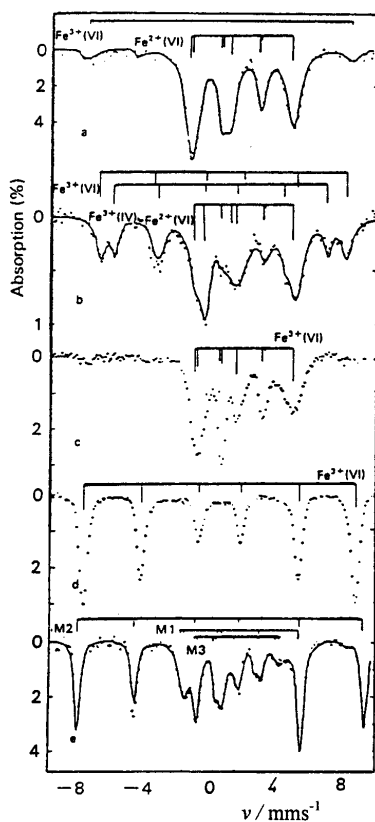


Fig. 32 Magnetic hyperfine splitting in induced pattern, recorded at 4.2 K, of greenalite (a), minnesotaite (b), ferripyrophyllite (c), crocidolite (d), and ilvaite (e) [49].

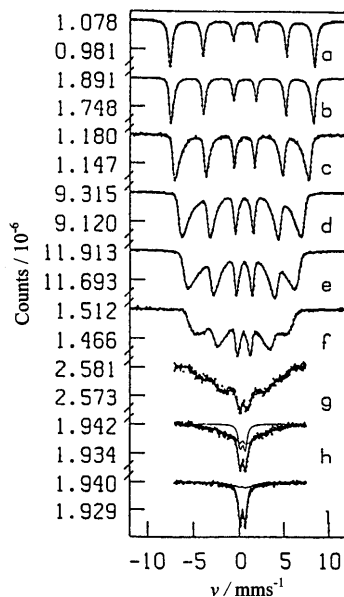


Fig. 33 Induced pattern of dark-brown limonite [53] at (a) 7 K, (b) 78 K, (c) 170 K, (d) 235 K, (e) 271 K, (f) 298 K, (g) 318 K, (h) 328 K, and (j) 340 K.

Table 6 (a) Ferrous hyperfine parameters for silicate minerals at 4.2 K [47].

| Mineral | Site | B/T | $\delta/\text{mm s}^{-1}$ | $\xi/\text{mm s}^{-1}$ | η |
|------------------|-------|-------|---------------------------|------------------------|--------|
| Greenalite | | 15.8 | 1.30 | -2.96 | 0.0 |
| Cronstedtite | | 14.1 | 1.39 | -2.77 | 0.2 |
| Minnesotaite | | 13.0 | 1.35 | -3.09 | 0.1 |
| Biotite | M1/M2 | 15.0 | | -2.75 | 0.2 |
| Orthoferrosilite | M1 | 29.0 | 1.34 | -2.5 | 0.9 |
| | M2 | 11.3 | 1.29 | 1.6 | 0.6 |
| Crocidolite | M1 | 19.6 | 1.31 | -2.77 | 0.1 |
| | M3 | 10.1 | 1.31 | -2.95 | 0.3 |
| Fayalite | M1 | 32.3 | | 3.08 | 0.2 |
| | M2 | 12.0 | | 3.02 | 0.2 |
| Laihunite | M1 | 26.0 | 1.32 | 2.9 | 0.0 |
| Almandine | | 22.8 | 1.39 | -3.45 | 0.1 |

(b) Ferric hyperfine parameters for silicate minerals at 4.2 K [47].

| Mineral | Site | B/T | $\delta/\text{mm s}^{-1}$ | $\varepsilon/\text{mm s}^{-1}$ |
|-------------------|------|-------|---------------------------|--------------------------------|
| Cronstedtite | IV | 40.6 | 0.35 | -0.13 |
| | VI | 46.7 | 0.54 | -0.14 |
| Ferripyrophyllite | M2 | 51.7 | 0.48 | 0.03 |
| Crocidolite | M2 | 55.0 | 0.52 | 0.17 |
| Laihunite | M2 | 50.5 | 0.50 | 0.3 |
| Ilvaite | A | 50.5 | 0.58 | 0.51 |

* $\xi = ce^2QV_{33}/(2E_0)$; η is the asymmetry parameter defined by eq. 5; $\varepsilon = \xi(3 \cos^2 \vartheta - 1)/4$; ϑ is the angle between the directions of V_{33} and \mathbf{B} .

temperature increases. (Note that the peaks have a steeper slope on the outer side than on the inner side.) An effective magnetic flux density $B = 49.7$ T (extrapolated to $T = 0$ K) and a transition temperature $T_N = 323$ K has been determined from the Mössbauer spectra. As opposed to the traditional interpretation (based on superparamagnetism), the temperature dependence of the spectra was interpreted in the frame of a relaxation model [51] involving magnetic ordering of clusters in which the cluster moments slowly relax, thus producing a Boltzmann distribution in the z component of the magnetization. Within a small grain, several clusters are created by high local concentrations of vacancies or other diamagnetic defects, and the cluster size varies with the temperature [52].

Magnetic relaxation effects have also been observed with olivines, $(\text{Mg}_{2-x}\text{Fe}_x)\text{SiO}_4$, as a function of x [54].

3.3.5 Grain size determination

The grain size distribution of ferromagnetic and antiferromagnetic iron minerals, oxides, and other compounds can also be determined by Mössbauer spectroscopy. This application has also proved to be important in other fields (e.g., archaeology, fine arts, etc.).

Figure 34 shows the room temperature spectra of hematite ($\alpha\text{-Fe}_2\text{O}_3$) samples of different grain size. The spectral differences reflect superparamagnetism, a phenomenon that can be observed with small ferromagnetic and antiferromagnetic grains behaving like huge paramagnetic particles. Grain size, namely, influences the relaxation time of the paramagnetic spin fluctuation [15,17,52]

$$\tau = \tau_0 \exp \frac{2KV}{kT} \quad (38)$$

where K is the anisotropy constant and V is the grain volume. Because of this, the hyperfine splitting of a ferromagnetic or antiferromagnetic grain may disappear provided that the grain is small enough for

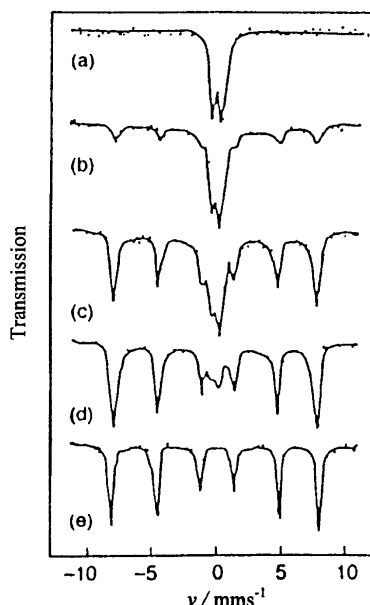


Fig. 34 Room-temperature Mössbauer spectra of hematite of different grain size [20]. (a): 10 nm, (b): 13.5 nm, (c): 15 nm, (d): 18 nm, and (e): 50 nm. The doublet (a) indicates that the 10-nm hematite particles are totally superparamagnetic, while 50-nm hematite particles show magnetic splitting (e) owing to antiferromagnetism.

the given temperature. Since τ is also the function of the temperature T , the size distribution can be determined from the temperature dependence of the Mössbauer pattern (Fig. 35).

The critical grain volume V_{sup} corresponding to the transition state (i.e., when the magnetic splitting just disappears in the spectrum) can be expressed by

$$V_{\text{sup}}(T) = \frac{kT}{2K} \ln \frac{\tau_{\text{sup}}}{\tau_0} \quad (39)$$

as the function of the temperature.

Note that by plotting the relative area (A) of the magnetically split subspectrum vs. the critical particle volume (V_{sup})—the latter being determined by the temperature of the measurement—we get the graph of the normalized distribution function F of the grain volume distribution:

$$F(V_{\text{sup}}) = A(V_{\text{sup}}) \quad (40)$$

from which the density function f can be obtained by differentiation

$$f(V_{\text{sup}}) = \frac{dA(V_{\text{sup}})}{dV_{\text{sup}}} \quad (41)$$

It is also important in many analytical applications that the temperature dependence of the spectrum may indicate whether a component represents superparamagnetic state or not.

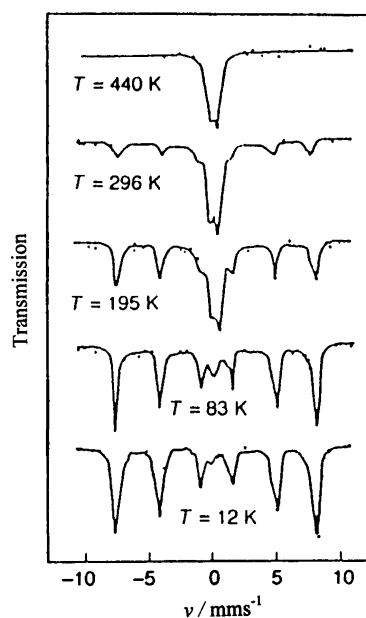


Fig. 35 Temperature dependence of the Mössbauer pattern of a superparamagnetic hematite sample [20].

3.4 Transformed pattern—amorphous and poorly crystallized state

Mössbauer spectroscopy is a unique tool for the investigation and characterization of minerals in amorphous or poorly crystallized state for which conventional diffraction methods fail. Important information on chemical bonding and short-range order in amorphous minerals has been obtained.

Several Mössbauer studies have been reported on obsidians and tektites that are typical amorphous natural substances. Figure 36 shows the standard and induced patterns of obsidian from Mt. Fuji, Japan [56].

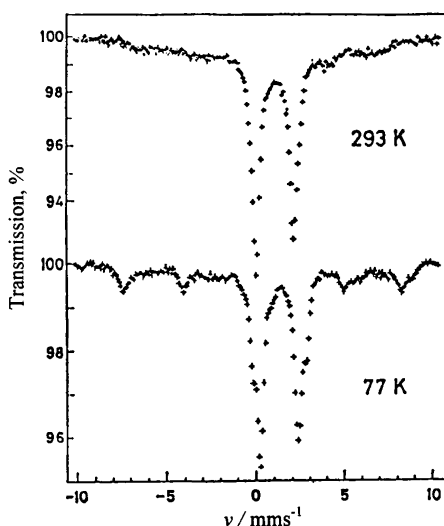


Fig. 36 Standard (a) and induced (b) patterns of obsidian, recorded at 293 K and 77 K, from Mt. Fuji [56]. The spectra could have been better analyzed by extracting the magnetic flux density and quadrupole splitting distributions (transformed patterns).

As an example for the application of Mössbauer spectroscopy for X-ray amorphous minerals, Fig. 37 shows routine Mössbauer spectra of opal samples from different Hungarian and Ukrainian localities. The samples are of different colors (black, green, greenish-yellow). There are no traces of inclusions or other fine-grained guest phases that may cause the color. According to the chemical analysis, the low iron content (0.1–1.0 %) is the only impurity that may be responsible for the color. The spectra demonstrate clearly that iron is present only in trivalent form, so that the theoretical calculations for possible oxygen–iron charge-transfer processes (as the main reason for different colors) should be based on trivalent iron [57].

Examples for the characterization of poorly crystallized minerals and minerals of very fine grain size have been shown previously in this section.

On grounds of the abundance of microenvironments in the amorphous and microcrystalline minerals as compared to regular crystalline ones, the authors strongly recommend to make use of transformed patterns, which can help classify elementary patterns, thus making it easier to identify the fingerprints of families of related microenvironments.

There exist improved softwares for deriving transformed patterns like hyperfine field (i.e., effective magnetic flux density) or quadrupole splitting distributions [24,27]. Such programs can consider/determine the relationship/correlation between the Mössbauer parameters (isomer shift–quadrupole splitting, isomer shift–hyperfine field, quadrupole splitting–hyperfine field).

The Mössbauer spectra of lunar soils reflect how the phase composition of soils depends on the locality where the samples were found. The main constituents of lunar soil are glassy agglomerates that

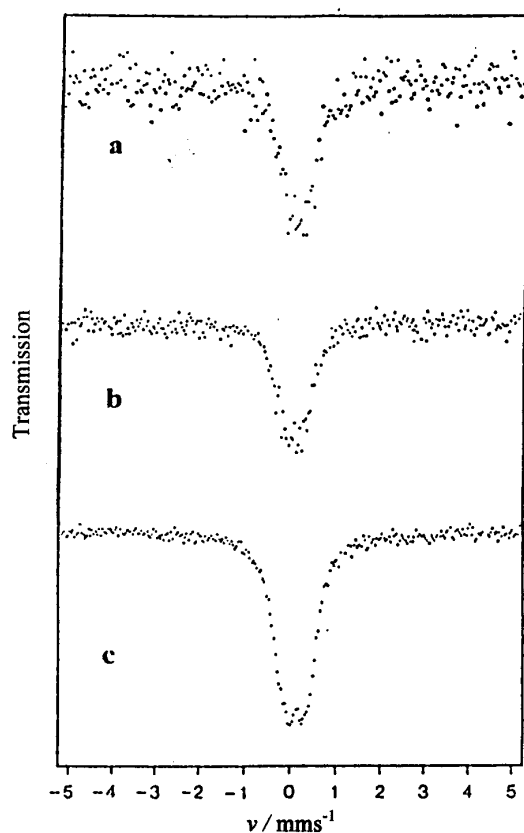


Fig. 37 Standard patterns of opals. (a) Black opal from Telkibánya, Hungary, (b) green opal (“ungvarite”) from Uzhgorod (Ungvár), Ukraine, (c) yellowish-green weathered opal from Monok, Hungary [57].

consist of composite particles agglutinated by inhomogeneous vesicular glass, and isolated homogeneous and inhomogeneous glass fragments with a wide range of color and transparency and with angular, ellipsoidal, or spherical shapes, or formed like dumbbells. Some glass particles show devitrification or inclusion of partially molten crystals. Additional components of the soil are isolated mineral particles of plagioclase, pyroxene, ilmenite, and olivine or fragments of rocks [58].

Figure 38 shows a typical Mössbauer spectrum of lunar soil. The absorption in the speed range between 0 and 3 mm/s results primarily from iron in silicate glass, pyroxene, and olivine. The peaks at lower and higher Doppler speeds are due to metallic iron. Table 7 shows the relative amount of iron in ilmenite to that in silicate in different lunar soil samples measured by Mössbauer spectroscopy [59].

The 300 K and 77 K Mössbauer spectra of glass particles separated from a lunar soil (Fig. 39) exhibit doublets due to Fe^{2+} ions in two distinct positions corresponding to the M1 and M2 position of pyroxene, reflecting a certain degree of devitrification [59]. FeTiO_3 has also been identified in the samples.

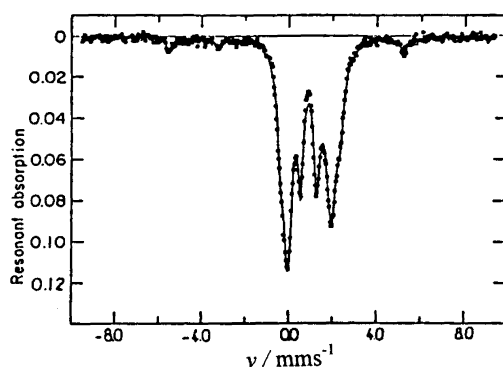


Fig. 38 Standard pattern of lunar soil [59]. Silicate glass, pyroxene, olivine, and α -iron can be identified from the spectrum decomposition.

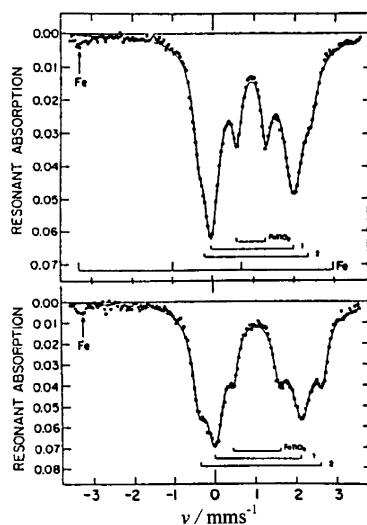


Fig. 39 Standard (upper) and induced (lower) patterns of lunar glass particles [59]. (The latter spectrum was taken at 77 K.) 1 and 2 denote the M1 and M2 sites in pyroxene. The spectra also reflect ilmenite and α -iron.

Table 7 Mössbauer hyperfine parameters of lunar glasses

| Sample color | Component no. | Interpretation | $\delta/\text{mm s}^{-1}$ | $\Delta/\text{mm s}^{-1}$ | $W/\text{mm s}^{-1}$ | Assymetry | Area (in %) |
|----------------|---------------|----------------|---------------------------|---------------------------|----------------------|-------------------|--------------------|
| Green | 1 | M1 | 0.960 ± 5 | 1.109 ± 11 | 0.576 ± 26 | 0.952 ± 12 | 53.5 ± 3.0 |
| | 2 | M2 | 0.896 ± 7 | 0.803 ± 16 | 0.628 ± 29 | | 46.5 ± 3.0 |
| Brown-greenish | 1 | M1 | 1.006 ± 7 | 1.170 ± 15 | 0.593 ± 35 | 0.986 ± 15 | 46.9 ± 3.4 |
| | 2 | M2 | 0.938 ± 8 | 0.860 ± 16 | 0.643 ± 30 | | 53.1 ± 3.4 |
| Green-brownish | 1 | M1 | 1.015 ± 12 | 1.251 ± 19 | 0.527 ± 53 | 0.937 ± 11 | 28.3 ± 3.5 |
| | 2 | M2 | 0.941 ± 8 | 0.914 ± 16 | 0.704 ± 31 | | 71.7 ± 3.5 |
| Gray-brownish | 1 | Olivine | 1.062 ± 12 | 1.500 ± 22 | 0.275 ± 59 | 1.045 28 | 18.4 ± 7.9 |
| | 2 | M1 | 1.033 ± 13 | 1.349 ± 48 | 0.345 ± 166 | | 17.7 ± 11.1 |
| | 3 | M2 | 1.026 ± 8 | 0.995 ± 29 | 0.666 ± 51 | | 63.9 ± 0.6 |
| Gray-brownish | 1 | Olivine | 1.053 ± 5 | 1.492 ± 11 | 0.279 ± 32 | 0.971 12 | 25.9 ± 5.6 |
| | 2 | M1 | 1.036 ± 7 | 1.336 ± 37 | 0.394 ± 78 | | 23.4 ± 7.2 |
| | 3 | M2 | 0.994 ± 7 | 0.966 ± 16 | 0.682 ± 32 | | 50.7 ± 6.0 |
| Black | 1 | M1 | 1.047 ± 6 | 1.253 ± 12 | 0.439 ± 27 | 1.010 ± 12 | 34.0 ± 2.2 |
| | 2 | M2 | 1.014 ± 3 | 0.969 ± 5 | 0.404 ± 12 | | 66.0 ± 2.2 |

The \pm values represent errors. If no decimal point is given, then the digits of the error refer to the digits right above them. For instance, the last data in the column of the isomer shift mean: $\delta = (1.014 \pm 0.003)$ mm/s.

3.5 Transformed pattern—crystalline state with a multitude of microenvironments

Transformed patterns can also be very useful for the interpretation of the complex spectra of regular crystalline minerals containing various cations that can substitute for each other, thus creating a multitude of slightly different microenvironments of the Mössbauer probe atom. No wonder that the spectral decomposition of such spectra to only a few elementary patterns cannot be performed unambiguously [63].

As an example, we refer to the glauconite sample whose standard pattern is shown in Fig. 40. The paramagnetic spectrum shown is very complex and may contain many subspectra. Owing to the high correlation of the peak parameters of the overlapping spectrum peaks, conventional spectrum analysis (i.e., the decomposition of the Mössbauer spectrum to a few quadrupole-split subspectra of Lorentzian peaks) cannot lead to an unambiguous solution. The result of the evaluation procedure depends, first of all, on the actual number of the different iron positions (each thought to be represented by a quadrupole doublet) that can be distinguished by Mössbauer spectroscopy. The number of subspectra can well be different from the exact number of crystallographic iron sites, because different microenvironments of the same site (e.g., having different cation neighborhoods) can also be distinguished by the Mössbauer method. The presence of numerous microenvironments can make the conventional evaluation unreli-

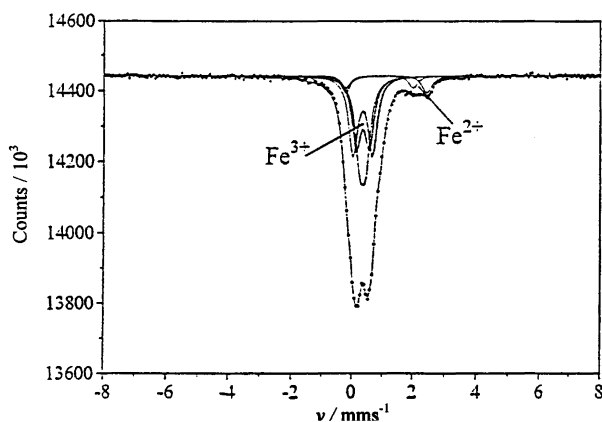


Fig. 40 The standard pattern of a glauconite sample [62].

able. In such a case, we can still use the quadrupole splitting distribution extracted from the Mössbauer spectrum. The peaks of the distribution curve can then be assigned to different microenvironments.

The former conventional trials aiming the evaluation of Mössbauer spectra were based on the decomposition to several doublets having Lorentzian peak shape. Different authors suggested different site assignments for the doublets depending on the number of doublets (3–6) used for the decomposition. In the case of the four-doublet fits, one of the interpretation assigns the doublets with isomer shifts and quadrupole splitting $\delta = 1.14$ mm/s, $\Delta = 2.60$ mm/s and $\delta = 0.35$ mm/s, $\Delta = 0.47$ mm/s to Fe^{2+} and Fe^{3+} in *cis* position, respectively, while the doublet with $\delta = 1.05$ mm/s, $\Delta = 2.15$ mm/s and $\delta = 0.56$ mm/s, $\Delta = 0.88$ mm/s to Fe^{2+} and Fe^{3+} in *trans* position, respectively [60]. Based on this site assignment, geological conclusion was drawn on the evolution of glauconite-bearing strata [61]. However, this site assignment for the glauconite, which is analogous to that used for trioctahedral micas, gives contradictory results concerning the temperature dependence of Mössbauer parameters. Another site assignment supposed that Fe^{3+} only occurs in *cis* position but with different neighborhoods characterized by binomial distribution in the second coordination shell within the octahedral sheet.

The authors of this paper calculated the transformed patterns (quadrupole splitting distributions) for a series of glauconites originating from Transylvania [62]. The analysis of the transformed pattern of glauconite helped to give a better explanation for the Mössbauer spectra. Figure 41 shows the transformed pattern of a glauconite sample. The peaks and subpeaks can be assigned to different micro-

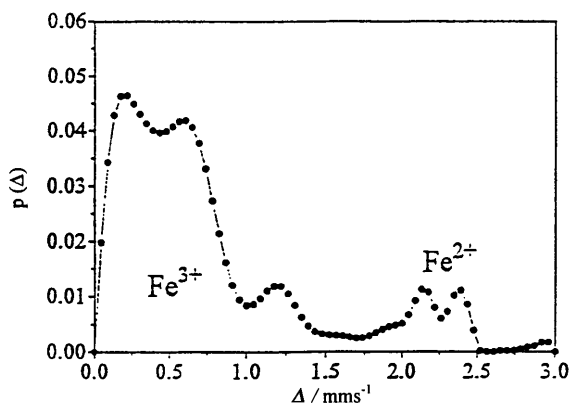


Fig. 41 The transformed pattern (quadrupole splitting distribution) of a glauconite sample [62].

environments as follows: Fe^{3+} *cis* position having different cation second neighborhood, Fe^{3+} in *trans* position, Fe^{2+} in *trans* position, and Fe^{2+} in *cis* positions.

The results [62] concerning the serial evaluation of spectra measured at different temperatures seem to indicate that the above interpretation was an essential step toward the final understanding and identifying of the glauconite microenvironments.

3.6. Analysis of meteorites

Mössbauer spectroscopy has given a fundamental contribution to the discovery of a new phase in the Fe–Ni alloys of meteorites [51]. The physical properties of this new phase have been found to depend on the cooling rate and other thermal conditions experienced by meteorites [51].

The Fe–Ni (50–50 %) alloy can exist as an ordered phase (with the superstructure L1_0) at temperatures below the critical order–disorder transition of $T_c = 539$ K. Owing to the extremely slow diffusion rate below this temperature, it has not been possible to obtain the ordered phase by thermal annealing. This phase has never been observed with terrestrial samples. The ordered phase has a small tetragonal distortion ($c/a = 1.0036$), and for this reason it has been referred to as tetrataenite after its discovery in meteorites [64]. Typical Mössbauer spectra of taenite from iron meteorites are shown in Fig. 42.

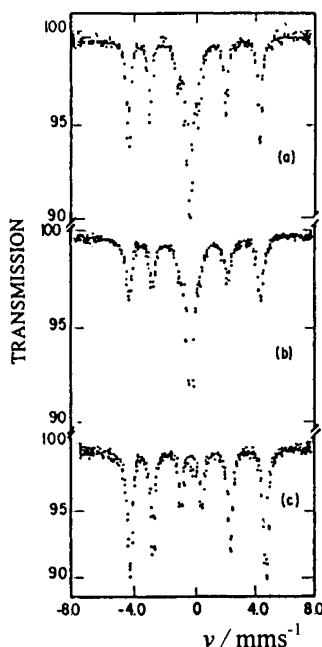


Fig. 42 Mössbauer spectra of taenite from meteorites [51], (a) Toluca, (b) Santa Catherina, and (c) Saint Severin.

Detailed analysis of the room-temperature Mössbauer spectrum (Fig. 43 and Table 8) of an Fe–Ni (92.5 % Fe, 7.5 % Ni) meteorite from Henbury, northern Australia, shows that it can be considered as a solid solution of Ni in iron. The peak broadening reflects a range of possible microenvironments [65] as discussed below. The distribution of hyperfine fields (effective magnetic flux density) in the meteorite sample is considered to reflect the slightly different atomic environments of the iron atoms due to the presence of Ni and trace atoms.

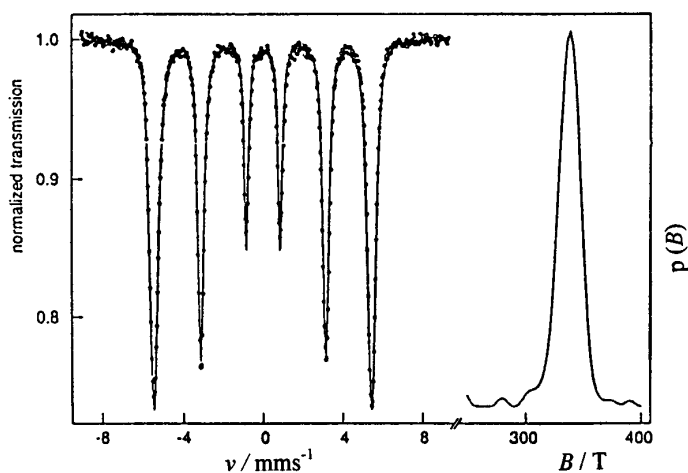


Fig. 43 Standard (left) and transformed (right) patterns of a meteorite sample [65].

Table 8 Comparison of the results for the meteorite sample with values for an $\text{Fe}_{0.925}\text{Ni}_{0.075}$ alloy.

| Mössbauer parameter | Meteorite (transmission integral fit) | Meteorite (distribution method [13]) | $\text{Fe}_{0.925}\text{Ni}_{0.075}$ |
|---------------------------|---------------------------------------|--------------------------------------|--------------------------------------|
| \bar{B}/T | 33.77 | 34.0 | 33.78 |
| $\Delta\bar{B}/T$ | | 2.3 | |
| $\delta/\text{mm s}^{-1}$ | 0.018 | 0.018 (fixed) | 0.023 |

The Mössbauer spectrum of a random iron-based alloy [40] can be considered as a set of a finite number of discrete components (elementary patterns) belonging to different alloying element configurations. It has been observed that in iron-based alloys the magnetic flux density at the nucleus of a host iron atom is approximately a linear function of the numbers of sites occupied by the alloying elements in the first and the second coordination sphere. The magnetic flux density can be expressed as:

$$B = B_0 + \sum_k (n_{1,k} \Delta B_{1,k} + n_{2,k} \Delta B_{2,k}) \quad (42)$$

where B_0 is the magnetic flux density experienced by iron nuclei, the first two neighborhoods of which contain only iron atoms, $n_{i,k}$ is the number of atoms of the k^{th} alloying element in the i^{th} coordination sphere, and $\Delta B_{i,k}$ is the increment of magnetic flux density caused by the k^{th} element situated in the i^{th} coordination sphere.

By supposing a random (binomial) distribution of elements with known concentration in the alloy, the numbers of alloying atoms situated in different surroundings can be calculated. On the other hand, by measuring the spectral areas of the components (each of which being proportional to the number of iron atoms having one particular microenvironment), the concentrations of the alloying elements can be determined. For this purpose, the use of transformed patterns (hyperfine field distribution) gives more accurate results than the simple Lorentzian decomposition of the spectrum [40].

3.7 Phase analysis of rocks

Ideally, the phase analysis of a rock should be performed according to the following strategy:

- (1) Etalons and studied samples: Standard and induced patterns are to be recorded at different points of the space of the externally adjustable experimental parameters (parameter space).
- (2) Etalons and studied samples: Transformed patterns are to be extracted from the spectra (natural patterns), and elementary patterns are to be determined.
- (3) Etalons: Since the fingerprint of any phase (at any point of the parameter space) can be interpreted as the weighted sum/integral of elementary patterns obtained in step 2, such weights are to be determined as a multivariate function in the parameter space.
- (4) Studied samples: The weight functions derived in step 3 can be used for building up the fingerprints of possible phases that are looked for in the given sample.

The following examples demonstrate the importance of the determination of induced and transformed patterns in the analysis of geological samples. (A detailed review of the field has been published elsewhere [63].)

In pure crystalline hematite, $\alpha\text{-Fe}_2\text{O}_3$, there is only one single microenvironment represented by a well-defined crystallographic position of Fe^{3+} . Accordingly, the standard pattern of the pure material is characterized by typical Mössbauer parameters. However, a careful systematic analysis of induced patterns is needed to identify the same mineral in a multiphase rock, since substitutional effects—or the effect of the nearby silicate surroundings—can cause changes in the microenvironments as demonstrated by Table 9 [66].

Similar conclusions can be drawn for the analysis of FeOOH . Table 10 [66] shows the Mössbauer data of natural and pure goethite samples. As we can see, there is a great variation in the parameter values depending on the origin of this mineral.

In magnetite, Fe_3O_4 , one can only find Fe^{3+} at the tetrahedral A site, while the octahedral B site contains both Fe^{3+} and Fe^{2+} . However, only two typical elementary patterns can be distinguished above 120 K, because the fast electron hopping at the B site smears out the observation of the separate microenvironments. However, below the Verwey transition, several magnetically split B-site patterns [32,67] can be observed, which can be used for the better identification of magnetite in rocks.

The detection limit of maghemite in basalt can be enhanced if the Mössbauer measurement is performed in an external magnetic field [68], because the elementary patterns of the individual sublattices can be distinguished owing to magnetic interaction (Figs. 44 and 45).

In the case of sediment samples taken from the River Elbe, Mössbauer spectroscopy has been used for the identification of the iron species (Fig. 46) [69].

Figure 47 [32] illustrates how important it is to find the appropriate external parameters at which the induced spectra are measured for the identification of different hydrous iron oxides in clay minerals [67]. Note that the predominant ferrihydrite phase ($5\text{Fe}_2\text{O}_3 \cdot 9\text{H}_2\text{O}$) could not be identified from the standard pattern of illite alone.

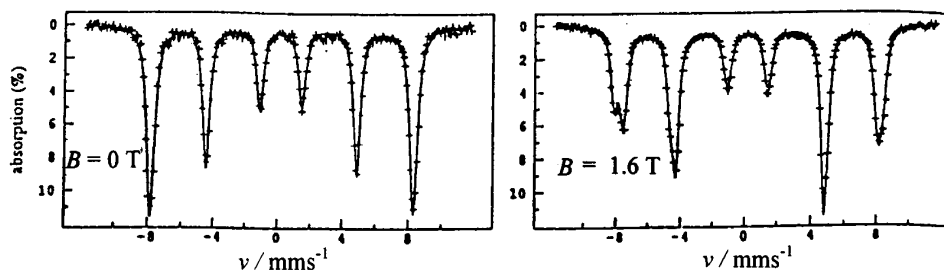


Fig. 44 Standard and induced patterns of pure maghemite with and without external magnetic field, respectively [68].

Table 9 Mössbauer parameters of Fe₂O₃.

| Substance | T/K | $\delta^a/\text{mm s}^{-1}$ | $\Delta/\text{mm s}^{-1}$ | B/T |
|--|-----------------|-----------------------------|---------------------------|-------------------|
| $\alpha\text{-Fe}_2\text{O}_3$ | 298 | 0.38 | -0.24 | 51.5 |
| | RT ^b | 0.367 | | |
| | →0 | | | 54.4 |
| | 296 | 0.39 | -0.21 | 51.8 |
| | 83 | | +0.35 | 54.2 |
| (18.0 nm, on SiO ₂) | 296 | 0.38 | -0.22 | 50.3 |
| | 80 | | -0.20 | 52.7 |
| (0.8 % Fe on SiO ₂) | RT | 0.36 | 0.84 | 0 |
| (0.9 % Fe on $\alpha\text{-Al}_2\text{O}_3$) | RT | 0.32 | 0.71 | 0 |
| (12 % Fe ₂ O ₃ on SiO ₂) | RT | | | 49.6 ^c |
| $\alpha\text{-(Fe}_{1-x}\text{Al}_x)_2\text{O}_3$ | | | | |
| $x = 0.0$ | RT | 0.43 | -0.17 | 51.5 |
| 0.1 | RT | 0.47 | -0.21 | 50.4 |
| 0.23 | RT | 0.48 | -0.25 | 49.4 |
| 0.901 | RT | 0.31 | 0.51 | 0 |
| 0.965 | RT | 0.27 | 0.43 | 0 |
| 0.67–0.90 | RT | 0.27 | 0.45 | 0 ^d |
| 0.99 | RT | | 0.837, 1.310 | 0 |
| 0.173 | RT | | | 50.5 |
| 0.16 | RT | 0.37 | -0.21 | 48.8 |
| | 77 | 0.35 | -0.22 | 52.4 |
| | 4 | 0.37 | -0.17 | 52.3 |
| $\alpha\text{-(Fe}_{1-x}\text{Rh}_x)_2\text{O}_3$ | | | | |
| $x = 0.0$ | 20 | 0.48 | 0.39 | 54.0 |
| 0.2 | 20 | | | 53.0 |
| 0.4 | 20 | | | 52.1 |
| 0.8 | 20 | | 0.26 | 47.0 |
| $\gamma\text{-Fe}_2\text{O}_3$ | RT | 0.27, 0.41 | 0 | 48.8, 49.9 |
| (9.3 nm) | 77 | | | 48.3, 50.8 |
| (800 × 135 nm) | 77 | | | 50.8, 52.5 |
| | RT | | 0.01 | 50.0 |
| | 4 | | 0.035 | 52.5 |
| $\beta\text{-Fe}_2\text{O}_3$ | 295 | 0.32, 0.33 | 1.44, 1.94 | 0 |
| | 4 | | | 49.6, 51.9 |
| | >300 | 0.31 | 1.0 | 0 |
| | 4 | | | 49.5 |
| $\epsilon\text{-Fe}_2\text{O}_3$ | 4 | 0.55 | 0.4 | 50.0 |

^aThe isomer shift is given relative to $\alpha\text{-Fe}$.^bRT means room temperature (about 293 K).^cA doublet has also been observed.^dMagnetic sextet has also been observed in varying proportions.

Table 10 Mössbauer parameters of FeOOH

| Substance | <i>T</i> /K | δ^a /mm s ⁻¹ | Δ /mm s ⁻¹ | <i>B</i> / <i>T</i> | |
|-----------------|------------------|--------------------------------|------------------------------|----------------------------|-------------------|
| α -FeOOH | 300 | – | – | 36.0 ± 1.5 | |
| | 110 | – | – | 52.0 ± 1.5 | |
| | RT ^b | 0.44 | – | 36.4 ± 4.0 | |
| | 77 | – | – | 51.5 ± 4.0 | |
| | (natural sample) | 295 | | 0.14 | 38.8 |
| | | 77 | | – | 50.4 |
| | (20 nm) | 295 | | 0.36 | 0 |
| | | 77 | | – | 48.9 ^c |
| | | RT | 0.35 | –0.3 | 38.3 |
| | | 77 | | –0.3 | 50.4 |
| (fine grain) | 4 | | –0.3 | 50.4 | |
| | RT | 0.37 | 0.52 | 0 | |
| | 300 | 0.33 | 0.56? | 34.0 | |
| | 77 | | 0.64? | 49.0 | |
| | (natural sample) | RT | 0.41 | –0.32 | 38.1 |
| β -FeOOH | 300 | | – | 0 | |
| | 110 | | – | 49.0 ± 1.5 | |
| | RT | 0.34 | 0.62 | 0 | |
| | 77 | – | – | 46.6 ± 5.0 | |
| | >RT | 0.35 | 0.70 | 0 | |
| | →0 | | –0.21 | 47.5 ± 0.5 | |
| | 300 | 0.37 | 0.7 | 0 | |
| | 4 | – | – | 47.0 ± 1.0 | |
| | RT | 0.38 | 0.96 ^d | 0 | |
| | RT | 0.38 | 0.7 | 0 | |
| | →0 | – | – | 47.0 ± 1.0 | |
| | 77 | – | – | 49.0, 52.0 | |
| | (56 nm) | 300 | | 0.58, 0.59, 0.71, 0.83 | |
| 80 | | | –0.24 | 47.6 | |
| | | | –0.82 | 45.4 | |
| | | | –1.51 | 43.8 | |
| | | | 0 | 0 | |
| 4 | | | –0.08 | 48.8 | |
| | | | –0.72 | 47.9 | |
| | | | +0.03 | 45.6 | |
| γ -FeOOH | | 110 | | – | 0 |
| | | RT | 0.39 | 0.54 | 0 |
| | 77 | | 0.62 | 0 | |
| | RT | 0.30 | 0.55 | 0 | |
| | 4 | | <0.1 | 46.0 ± 0.5 | |
| (bulk) | RT | | 0.555 | 0 | |
| (1.0 nm film) | RT | | 0.94 | 0 | |
| δ -FeOOH | 77 | 0.36 | – | 53.3 ± 5.0 | |
| | RT | 0.38 | 0.48 | 0 | |
| | 83 | | 0.47 | 51.9 | |
| | (fine grain) | RT | 0.31 | 0.48 | 0 |
| | 80 | | –0.1 | 52.5 (oct.) 50.5 (tet.) | |

(continued on next page)

Table 10 (Continued).

| Substance | <i>T</i> /K | δ^a /mm s ⁻¹ | Δ /mm s ⁻¹ | <i>B</i> /T |
|-----------------------|-------------|--------------------------------|------------------------------|-------------|
| FeOOH (high pressure) | 295 | 0.37 | -0.130 | 47.2 |
| | 10 | | -0.118 | 52.3 |

^aThe isomer shift is given relative to α -Fe.

^bRT means room temperature (about 293 K).

^cA doublet has also been observed.

^dTwo doublets have been observed.

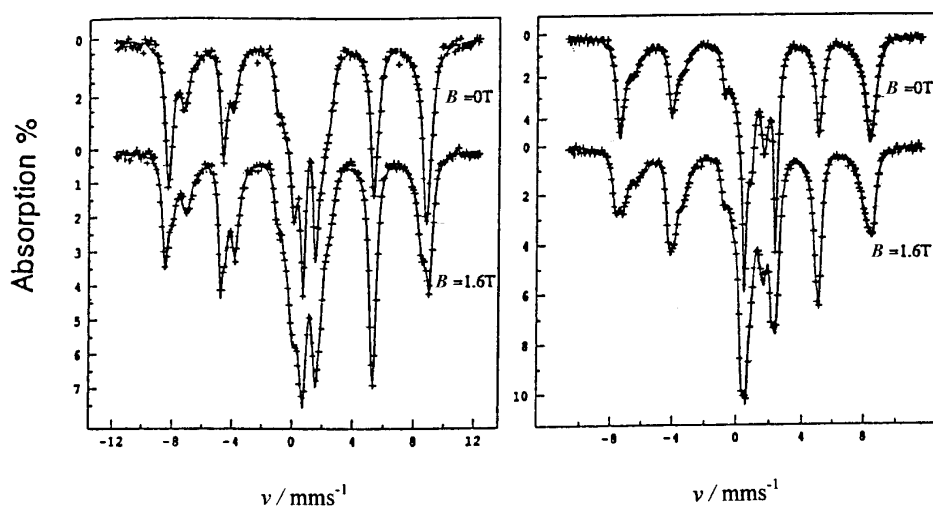


Fig. 45 Standard and induced patterns of two samples of different lava flows, with and without external magnetic field [68]. The presence of maghemite can be shown positively.

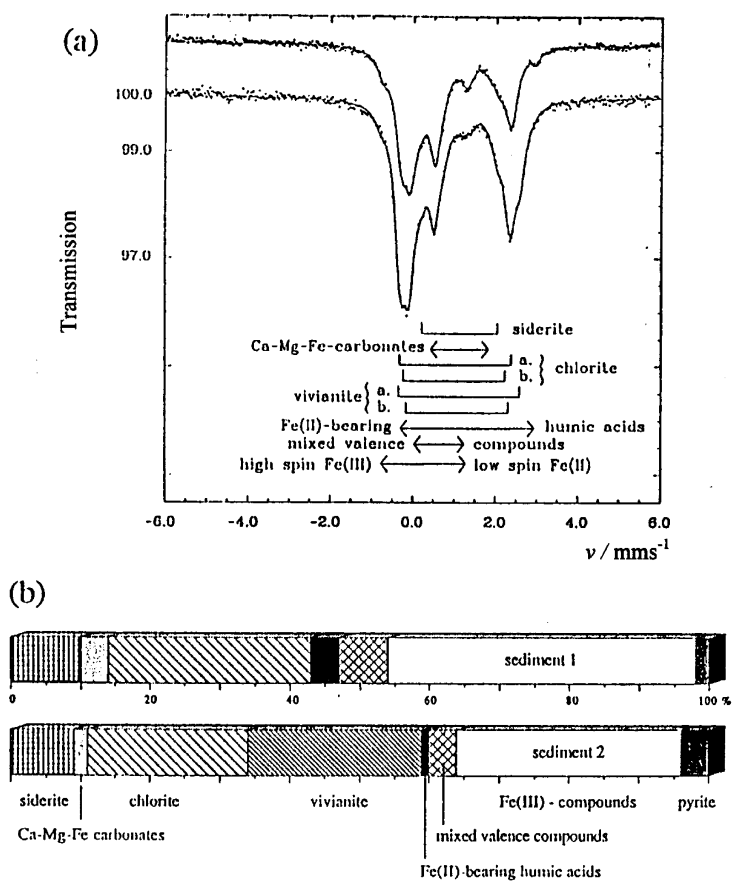


Fig. 46 Standard patterns of two sediment samples from the River Elbe (a). The distribution of iron between the fractions in the sediment samples (b). The spectrum analysis has been performed by the transmission-integral method [69].

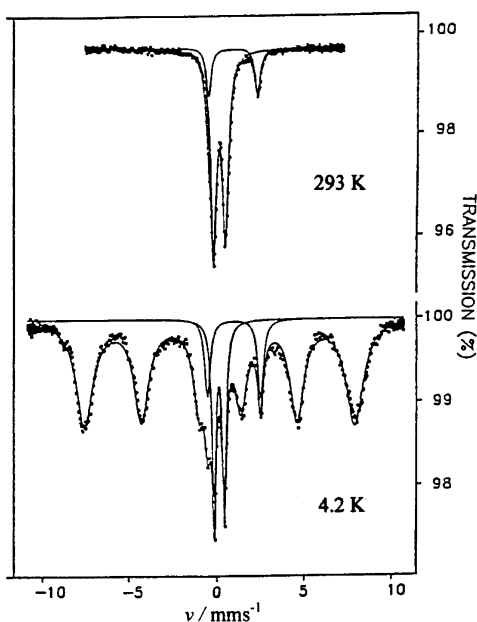


Fig. 47 Standard and induced patterns of an illite sample [32].

CONCLUSIONS

Any qualitative analysis based on Mössbauer spectroscopy boils down to identifying the individual physical or chemical species from the corresponding patterns present in the spectrum. Ideally, this can be done if we know the exact correspondence between patterns and species. Such a one-to-one correspondence between species of atoms and individual patterns, however, can be nonexistent for the given set of externally adjusted experimental parameters at which the Mössbauer spectrum is recorded. For this reason, it is useful to consider all the Mössbauer parameters (P_M) as a function of a number of externally adjustable experimental quantities such as the temperature (T), pressure (p), external magnetic flux density (B_{ext}), polar angles (θ , ϕ), frequency of high frequency field (ν), etc.:

$$P_M = f(T, p, B_{ext}, \theta, \phi, \nu, \dots)$$

However, when the whole range of these parameters is considered, we may find points in the space of experimental parameters at which only one pattern is associated with one species and vice versa, and thus we can get round the problem of ambiguity.

From the analytical point of view, we can introduce a useful terminology classifying Mössbauer patterns.

A Mössbauer pattern can be either a simple spectrum called **elementary pattern**, reflecting only a hyperfine interaction at one particular microenvironment, or a complex spectrum called **superimposed pattern** that consists of a number of subspectra. Here, we refer to a family of Mössbauer nuclei experiencing the same hyperfine interaction as a **microenvironment**.

A **standard pattern** is related to a Mössbauer spectrum that is measured at a standard set of externally adjusted experimental parameters. An **induced pattern**, on the other hand, is obtained under conditions other than standard. The differences between the induced and the spontaneous pattern can give important contribution to the analysis.

The **transformed pattern** is obtained from the measured Mössbauer spectrum (**natural pattern**) by mathematical transformation (e.g., by Fourier transformation). The magnetic hyperfine field (i.e., ef-

fective magnetic flux density) distribution and the quadrupole splitting distribution are transformed patterns. The transformed pattern may give a better resolution for the analysis.

Our approach can also contribute to the systematization of Mössbauer data for the identification of individual physical or chemical species from the corresponding patterns present in the spectrum.

The concept suggested in this paper can also be adapted to analytical methods other than Mössbauer spectroscopy.

Examples for the use of the terminology are given in the field of mineralogy and geology.

REFERENCES

1. R. L. Mössbauer. *Z. Physik* **151**, 124 (1958).
2. G. K. Wertheim. *Mössbauer Effect*, Academic, New York (1964).
3. N. N. Greenwood and T. C. Gibb. *Mössbauer Spectroscopy*, Chapman and Hall, London (1971).
4. V. I. Goldanskii and R. H. Herber. *Chemical Application of Mössbauer Spectroscopy*, Academic, New York (1968).
5. U. Gonser (Ed.). *Mössbauer Spectroscopy, Topics in Applied Physics*, Springer, Berlin (1975).
6. I. J. Gruverman (Ed.). *Mössbauer Effect Methodology*, Plenum, New York (1965).
7. L. May. *An Introduction to Mössbauer Spectroscopy*, Plenum, New York (1971).
8. G. K. Shenoy and F. E. Wagner (Eds.). *Mössbauer Isomer Shifts*, p. 106, North Holland, Amsterdam (1978).
9. H. Frauenfelder. *The Mössbauer Effect*, Benjamin, New York (1962).
10. H. Wegener. *Der Mössbauer Effekt und seine Anwendungen in Physik und Chemie*, Bibliographische Institut AG, Mannheim (1965).
11. P. Gütlich, R. Link, A. Trautwein. *Mössbauer Spectroscopy and Transition Metal Chemistry*, Springer, Berlin (1978).
12. T. C. Gibb. *Principles of Mössbauer Spectroscopy*, Chapman and Hall, London (1976).
13. G. M. Bancroft. *Mössbauer Spectroscopy*, McGraw Hill, London (1973).
14. B. V. Thosar, J. K. Srivastava, P. K. Iyengar, S. C. Bhargava (Eds.). *Advances in Mössbauer Spectroscopy*, Elsevier, Amsterdam (1983).
15. A. Vértes, L. Korecz, K. Burger. *Mössbauer Spectroscopy*, Elsevier, Amsterdam (1979).
16. C. Kittel. *Introduction to Solid State Physics*, Wiley, New York (1968).
17. A. Vértes and D. L. Nagy (Eds.). *Mössbauer Spectroscopy of Frozen Solutions*, Akadémiai Kiadó, Budapest (1990).
18. U. Gonser (Ed.). *Mössbauer Spectroscopy II. The Exotic Side of the Method*, Springer, Berlin (1981).
19. S. Nagy, B. Lévy, A. Vértes. *Acta Chim. Acad. Sci. Hung.* **85**, 273 (1975).
20. E. Kuzmann, S. Nagy, A. Vértes. "Mössbauer spectroscopy in chemical analysis". In *Chemical Analysis by Nuclear Methods*, Z. Alfassi (Ed.), Wiley, New York (1994).
21. J. M. D. Coey. "Mössbauer spectroscopy of silicate minerals". In *Mössbauer Spectroscopy Applied to Inorganic Chemistry*, G. J. Long (Ed.), Vol. 1, p. 443, Plenum, New York (1984).
22. B. Window. *J. Phys. E: Sci. Instrum.* **4**, 401 (1971).
23. J. Hesse and A. Rübartsch. *J. Phys. E: Sci. Instrum.* **7**, 526 (1974).
24. Z. Klencsár, E. Kuzmann, A. Vértes. *J. Rad. Nucl. Meth. Articl.* **210**, 105 (1996).
25. N. Seagusa and A. H. Morrish. *Phys. Rev.* **B26**, 10 (1982).
26. R. A. Brand and G. Le Caer. *Nucl. Instr. Meth.* **B34**, 272 (1988).
27. P. G. Rancourt. *Phys. Chem. Miner.* **21**, 244 (1994).
28. J. G. Stevens and V. E. Stevens. *Mössbauer Effect Data Index and Reference Journal*, Adam Hilger, London (1969).

29. J. G. Stevens, H. Pollak, Li Zhe, V. G. Stevens, R. M. White, J. L. Gibson (Eds.), *Mössbauer Handbook, Mineral References and Mineral Data*, Mössbauer Effect Data Center, Asheville, NC USA, (1983).
30. E. O. T. Salles, P. A. de Souza, Jr., V. K. Garg. *J. Radioanal. Nucl. Chem.* **139**, 439 (1995).
31. E. Kuzmann, S. Nagy, A. Vértes. *J. Radioanal. Nucl. Chem. Lett.* **186**, 463 (1994).
32. E. Murad. *Hyp. Int.* **117**, 39 (1998).
33. L. Heller-Kallai and I. Rosenson. *Phys. Chem. Miner.* **7**, 223 (1981).
34. F. C. Hawthorn (Ed.), "Mössbauer spectroscopy," in "Spectroscopic Methods in Mineralogy and Geology", *Rev. Mineral.* **18**, 279 (1988).
35. G. Amthauer, H. Annerstein, S. S. Hafner. *Z. Kristallogr.* **143**, 14 (1976).
36. R. G. Burns. *Mineralogical Applications of Crystal Field Theory*, Cambridge University Press, Cambridge (1970).
37. G. M. Bancroft, A. G. Maddock, R. G. Burns. *Geochim. Cosmochim. Acta* **31**, 2219 (1967).
38. P. G. L. Williams, G. M. Bancroft, M. G. Brown, A. C. Turnock. *Nature* **230**, 149 (1971).
39. Z. Homonnay, E. Kuzmann, A. Vértes, A. Pákozdi, I. Kubovics, Cs. Szabó, G. K. Sóllymos, M. Jánosi. *Hyp. Int.* **57**, 2215 (1990).
40. S. Nagy, E. Kuzmann, A. Vértes, G. Szabó, G. Konczos. *Nucl. Instr. Meth.* **B34**, 217 (1988).
41. M. G. Clark, G. M. Bancroft, A. J. Stone. *J. Chem. Phys.* **47**, 4250 (1967).
42. L. P. Aldridge, G. M. Bancroft, M. E. Fleet, C. T. Herzberg. *Am. Mineral.* **63**, 1107 (1978).
43. S. Nagy, E. Szilágyi, Y. Wei, A. Nath. *Struct. Chem.* **1**, 297 (1990).
44. S. Mitra. *Applied Mossbauer Spectroscopy, Physics and Chemistry of Earth*, Vol. 18, Pergamon, Oxford (1992).
45. L. R. Walker, G. K. Wertheim, V. Jaccarino. *Phys. Rev. Lett.* **6**, 98 (1961).
46. D. M. Dyar. *Am. Mineral.* **72**, 102 (1987).
47. A. Moukarika, J. M. D. Coey, N. V. Dang. *Phys. Chem. Miner.* **9**, 269 (1983).
48. E. Murad and F. E. Wagner. *Phys. Chem. Miner.* **14**, 264 (1987).
49. J. M. D. Coey, O. Ballet, A. Moukarika, D. L. Soubeyroux. *Phys. Chem. Miner.* **7**, 141 (1981).
50. O. Ballet and J. M. D. Coey. *Phys. Chem. Miner.* **8**, 218 (1982).
51. J. Danon. "Applications of Mössbauer spectroscopy to study some minerals", Recent trends in: *Applications of Mössbauer Spectroscopy*, Yu. Kagan and I. Lyubutin (Eds.), p. 347, Gordon and Breach, New York (1985).
52. M. Blume and T. Tjon. *Phys. Rev.* **165**, 466 (1968).
53. D. A. Rice, J. D. Cashion, S. Bocquet. *Hyp. Int.* **91**, 697 (1994).
54. S. Bocquet, R. J. Pollard, J. D. Cashion. *Phys. Rev. B* **46**, 11657 (1992).
55. S. Bocquet and J. Kennedy. *J. Magn. Magn. Mater.* **109**, 260 (1992).
56. T. Tominaga and Y. Minai. *Nucl. Sci. Appl.* **1**, 749 (1984).
57. J. Takács. *Topographia Mineralogica Hungariae II*, 209 (1994).
58. S. S. Hafner. "Mössbauer spectroscopy in lunar geology and lunar mineralogy", in *Mössbauer Spectroscopy*, U. Gonser (Ed.), p. 167, Springer, Berlin (1975).
59. S. S. Hafner, B. Janik, D. Virgo. *Mössbauer Effect Methodology*, Vol. 6, I. J. Gruverman (Ed.), p. 193, Plenum, New York (1970).
60. L. Rosenson and L. Heller-Kallai. *Clays Clay Miner.* **23**, 289 (1978).
61. L. G. D. Mc Conchie, J. B. Ward, V. B. Mc Cann, D. W. Lewis. *Clays Clay Miner.* **27**, 339 (1979).
62. T. G. Weiszbarg, D. Pop, E. Kuzmann, S. Nagy, Z. Klencsár. *An. Inst. Geol. Roman.* **69**, 208 (1996).
63. E. Kuzmann, S. Nagy, A. Vértes, T. G. Weiszbarg, V. K. Garg. "Geological and Mineralogical Applications of Mössbauer Spectroscopy", in *Nuclear Methods in Mineralogy and Geology*, A. Vértes, S. Nagy, K. Süvegh (Eds.), pp. 285–376, Plenum, New York (1998).
64. R. B. Scorzelli. *Hyp. Int.* **66**, 249 (1991).
65. C. Bötter, S. J. Campbell, E. Wu, R. G. Smith. *Hyp. Int.* **91**, 563 (1994).

66. L. H. Bowen. *Mössbauer Effect Reference and Data Index*, J. Stevens (Ed.), p. 76 (1978).
67. E. Murad, J. H. Johnston. "Iron oxides and oxyhydroxides", in *Mössbauer Spectroscopy Applied to Inorganic Chemistry*, G. J. Long (Ed.), Vol. 2, pp. 507–583, Plenum, New York (1984).
68. Ö. Helgason, H. P. Gunnlangsson, S. Steinthorsson, C. Bender Koch, S. Morup. *Hyp. Int.* **91**, 583 (1994).
69. I. König and R. Hollatz. *Hyp. Int.* **57**, 2245 (1990).